HU ISSN 1785-6892 in print
HU ISSN 2064-7522 online

DESIGN OF MACHINES AND STRUCTURES

A Publication of the University of Miskolc

Volume 9, Number 1

Miskolc University Press
2019

EDITORIAL BOARD

Á. DÖBRÖCZÖNI
Editor in Chief
Institute of Machine and Product Design
University of Miskolc
H-3515 Miskolc-Egyetemváros, Hungary
machda@uni-miskolc.hu

Á. TAKÁCS
Assistant Editor
Institute of Machine and Product Design
University of Miskolc
H-3515 Miskolc-Egyetemváros, Hungary
takacs.agnes@uni-miskolc.hu

R. CERMAK
Department of Machine Design
University of West Bohemia
Univerzitní 8, 30614 Plzen, Czech Republic
rcermak@kks.zcu.cz

B. M. SHCHOKIN
Consultant at Magna International Toronto
borys.shchokin@sympatico.ca

W. EICHLSEDER
Institut für Allgemeinen Maschinenbau
Montanuniversität Leoben,
Franz-Josef Str. 18, 8700 Leoben, Österreich
wilfrid.eichlseder@notes.unileoben.ac.at

S. VAJNA
Institut für Maschinenkonstruktion,
Otto-von-Guericke-Universität Magdeburg,
Universität Platz 2, 39106 Magdeburg, Deutschland
vajna@mb.uni-magdeburg.de

P. HORÁK
Department of Machine and Product Design
Budapest University of Technology and Economics
horak.peter@gt3.bme.hu
H-1111 Budapest, Műegyetem rkp. 9.
MG. ép. I. em. 5.

K. JÁRMAI
Institute of Materials Handling and Logistics
University of Miskolc
H-3515 Miskolc-Egyetemváros, Hungary
altjar@uni-miskolc.hu

L. KAMONDI
Institute of Machine and Product Design
University of Miskolc
H-3515 Miskolc-Egyetemváros, Hungary
machkl@uni-miskolc.hu

GY. PATKÓ
Department of Machine Tools
University of Miskolc
H-3515 Miskolc-Egyetemváros, Hungary
patko@uni-miskolc.hu

J. PÉTER
Institute of Machine and Product Design
University of Miskolc
H-3515 Miskolc-Egyetemváros, Hungary
machpj@uni-miskolc.hu

CONTENTS

Alsarayefi, Saad–Ghafil, Hazim Nasir–Jálics, Károly: Optimisation of the fibre size for a Fiber Glass – Epoxy Composite 5

Mohamad, Barhm–Jálics, Károly–Zelentsov Andrei: Investigation and optimization of the acoustic performance of formula student race car intake system using coupled modelling techniques 13

Kiss, Róbert–Szilágyi, Attila: Analysis of the dynamic behaviour of the CNC machine centre by FEM 24

Klazly, Mohamad Mehi Alddin–Bognár, Gabriella: Computational fluid dynamic simulation of laminar flow over a flat plate 29

Kundrát, Tamás–Szilágyi, Attila: Finite element thermal simulation of a CNC milling machine 48

Kundrát, Tamás–Szilágyi, Attila: Thermovision analysis of a CNC milling machine 54

Szabó, Kristóf–Takács, György–Hegedűs, György–Tóth, Sándor Gergő: Examination of design methodology of screw conveyors 58

Takács, Ágnes: Generating concepts with mobile application 64

Design of Machines and Structures, Vol. 9, No. 1 (2019), pp. 5–12.
DOI: 10.32972.dms.2019.001

OPTIMISATION OF THE FIBRE SIZE FOR A FIBER GLASS – EPOXY COMPOSITE

SAAD ALSARAYEFI–HAZIM NASIR GHAFIL–KÁROLY JÁLICS

University of Miskolc, Department of Machine and Product Design
3515 Miskolc-Egyetemváros
machsa@uni-miskolc.hu

Abstract: In this paper, swarm intelligence optimisation algorithms are used to estimate the optimal size of the glass fibre of circular cross-section of a glass-epoxy composite. Finding the best fibre size in a composite material has significant benefits on cost reduction. A comparative study was done to select optimal fibre diameter that can satisfy the optimal longitudinal tensile strength. Particle swarm optimisation algorithm PSO and artificial bee colony algorithm ABC are proposed for this comparative study.

Keywords: *Optimisation, Composite material, Homogenisation*

1. INTRODUCTION

Fibre reinforced composite is a rapidly growing class of materials because of the importance of having low weight with high strength material. Mainly, polymer matrix reinforced with fibres, such as glass, carbon, or aramid is extensively used in almost all engineering sector applications. As a reinforcement, the fibre is the most commonly used with ceramics, metals, and polymers to have materials with the advantages of high strength, stiffness, toughness, wear and corrosion resistance, and reduced cost.

From this, and over decades, many works of literature have been done to investigate the influence of the size of different types of fibres on the overall characteristics of the composite materials. S. T. Pinho et al. [1] studied the effect of fibre size on the strength and toughness of fibre reinforced composite. F. Ramsteiner [2] investigated the influence of fibre diameter on the tensile behaviour of short-glass-fibre reinforced polymers. Hamdullah Çuvalci [3], has researched the effect of a glass fibre content on the mechanical properties of a composite material. These researchers and others have confirmed that the fibre diameter has significant effects on the mechanical characteristics of the composite materials.

Glass fibre reinforced plastic (GFRP), e.g. Glass fibre/Epoxy is a class of plastic matrix composites that is reinforced by glass to mechanically enhance strength and stiffness of plastics. The resin (matrix) supports the fiber and adds more protection because of its ability of providing bonding between the two materials. As a result, GFRP presents flexible option for structural design due to its accessibility of manufacturing, high durability and stractural efficiency (strength to weight ratio), and low production cost [4, 5]. Thus, the GFRP use has significantly expanded to the structural parts of airplanes, automobiles, marine, civil construction industries, sport goods.

Although, when designing composite materials, it is normal to take the matrix characteristics into account, in such cases, the essential factors which make changes in the material features are fibre size (diameter, length), fibre orientation, fibre contents and others [6]. This work studies the relationship between the fibre diameter (optimum) and the longitudinal tensile

strength when designing materials based on representative volume element (RVE) or a unit cell, using an optimisation algorithm.

2. MULTI SCALE APROACH

Traditionally, simulation models were developed for one specific scale of magnitude (macroscopic, microscopic or nano). In practice, it would be impossible to compute the vibration simulation for GFRP parts in the micro scale, because of the very fine calculation model and the resulting huge number of elements. The general idea of the multi-scale approach is to de-fine a context between models of different scales by reasonably linking results of adjacent scales. The multi-scale approach is widely used in science [7].

In this case the multi-scale method is used to derive the material properties (Young's modulus and density) in the macro-structure based on the detailed information in its micro-structure. The micro-structure corresponds to the scale in which heterogeneities can be modeled for several small and representative local sections of a part, while the macro structure of the part is modeled homogeneously with Young's modulus and density values differing among defined sections.

In the macro scale model, it is assumed that the properties of each material point (node of the macro model) can be described by mapping information from a representative volume element (RVE). This approach was firstly suggested by Drugan and Willis [8]. This RVE contains the information of underlying the inhomogeneous micro structure. Original material properties like Young's Modulus and density are used for a classical solid mechanic analysis of the inhomogeneous RVE. In a homogenization step substitute Young's Modulus and density are determined for the RVE based on the equivalence of stress and strain. These new substitute properties are called Boundary Conditions (BC) for macro nodes and are mapped to the relevant nodes of the macro scale model *(Figure 1).*

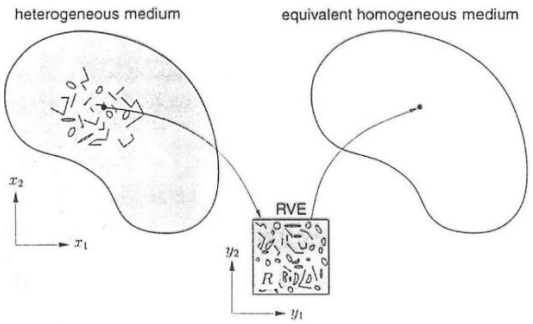

Figure 1. Overview of Multi-scale approach

A Mean-Field Homogenization (MFH) is used in this step, which is based on the relation between volume averages and stress or strain fields in each phase of a RVE. In first-order homogenization substitute materials are computed with real constitutive rules (constant volume, density and energy). A typical example of MFH is the Mori–Tanaka model [9] which is successfully applicable to two-phase composites with identical and aligned with ellipsoidal inclusions. The single inclusion problem (2D) was solved analytically by J. D. Eshelby [10]. 3D application has to be solved numerically (double inclusion problem). The model assumes

that each inclusion of the RVE behaves as if it was alone in an infinite body made of the real matrix material. The BCs in the double inclusion problem correspond to the volume average of the strain field in the matrix phase of the real RVE.

Depending on the possible periodic distribution of the fibre in the composite materials, the RVE or unit cell might be of square or hexagonal packing array as shown in *Figure 2* [11].

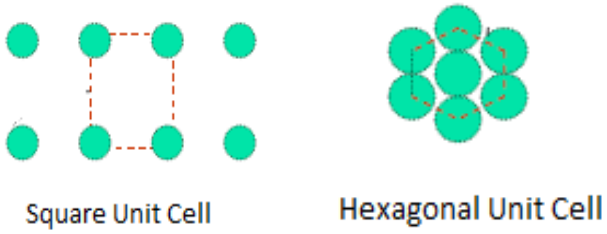

Figure 2. Schematic Representation of Unit Cells

In the theory of composite materials, the unit cell is modelled based on assumption such as the homogeneity of the composite material [11]. Taking into consideration the square unit cell with four fibre arrangement *(Figure 3)*, the longitudinal tensile strength can be calculated using the equation:

$$F1t = F_{ft}\left(v_f + \frac{E_m}{E_f}\right)(1 - v_f) \tag{1}$$

Where :
F_{1t}*: Longitudinal Tensile Strength*
F_{ft}*: Fiber Tensile Strength*
V_f*: Fiber Volume Fraction*
E_m*: Matrix Young's Modulus*
E_f*: Fiber Young's Modulus*

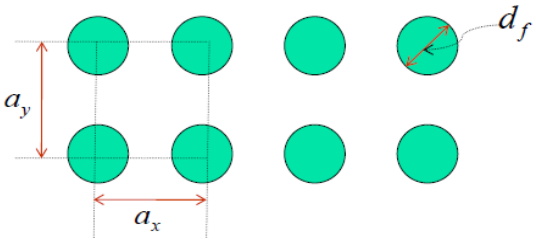

Figure 3. Square Unit Cell with Four-Fiber Arrangement

Since the volume fraction of the fibre is:

$$vf = \frac{\text{volume of the fiber}}{\text{total volume}} = \frac{\frac{\pi}{4}(df)^2}{ax.ay} \tag{2}$$

A direct relationship exists between the fibre and the longitudinal tensile strength.

3. CLASSIFICATION AND CHARACTERISTICS OF THE GLASS FIBER

The two phases of the material were chosen to be glass as fibre and epoxy as a matrix. The classifications of the most used glass fibers with their physical properties are shown below.

Table 1
Glass Fiber mail classes and the physical properties

Class of GF	Physical Properties
E-Glass	Higher strength and electrical resistivity
S-Glass	Highest tensile strength
R-Glass	Higher strength and acid corrosion resistance
C-Glass	Higher Corrosion resistance
D-Glass	Low dielectric constant

Based on *Equation (1)*, mechanical characteristics of the fibre and matrix are needed regardless of the fibre diameter which determines the volume of the fibre consequently by the fibre volume fraction vf. These characteristics are Ef, Em, and Fft. *Table 2* shows the required characteristics of the glass fiber.

Table 2
Glass Fiber Characteristics

Glass Fibre	***Ef, Gpa***	***Fft, Gpa***
E-Glass	72.35	3.45
S-Glass	85	4.8
R-Glass	86	4.4
C-Glass	69	3.31
D-Glass	55	2.5

4. CLASSIFICATION AND CHARACTERISTICS OF EPOXY

The contribution of epoxy resins in the composite material is by producing strength, durability, and chemical resistance. Their performance at elevated temperature with hot and wet service is high. Because of the outstanding adhesive ability that the epoxies have, they are able to bond very well with different types of fiber producing composite material with attractive properties. From this point, epoxies are taking a major part in the polymer matrix use for composite materials. Epoxy resin is widely used as a structural matrix in high-performance polymer composites for aeronautical and astronautical applications.

According to many literatures, epoxy resins are classified to many types. The table belw presents some types of epoxy as a matrix with their modulus of elasticity that required for *Equation (1).*

Table 3
Epoxy Characteristics

Epoxy	***Em, Gpa***
8551-7	4.098
8552	4.667
9310/9360 @23c	3.12
9310/9360 @149c	1.4
9420/9470 (A) @23c	2.66
9420/9470 (B) @23c	2.83
HPT1072/1062-M @23C	3.383

5. OPTIMISATION ALGORITHM

Particle swarm optimisation PSO [12] is a powerful and efficient optimisation algorithm which is widely used for a wide range of applications. PSO mimics the swarm behaviour of fish and birds, we can call the members of the swarm and the swarm itself as particles and population respectively, and every agent is a candidate solution to the optimisation problem. The position and velocity of a specific particle is denoted by

$$x_k(t) \in x$$
$$v_k(t) \in x$$

where *k* is the index of the agent in the swarm and *x* is the search area while (t) is the iteration number of the algorithm. The standard PSO is as follows

$$x_{kj}(t+1) = x_{kj}(t) + v_{kj}(t+1) \tag{3}$$

$$v_{kj}(t+1) = w * v_{kj}(t) + r_1 C_1 (p_{kj}(t) - x_{kj}(t)) + r_2 C_2 (G_j(t) - x_{kj}(t)) \tag{4}$$

$v_{kj}(t+1)$: denote the velocity of particle k in time step (t + 1) and the jth component for this velocity

r_1, r_2: a random number in the range 0 to 1

C_1,C_2: acceleration coefficient

w: inertia coefficient

$w * v_{kj}(t)$: inertia term

$r_1 C_1 (p_{kj}(t) - x_{kj}(t))$: cognitive component

$r_2 C_2 (G_j(t) - x_{kj}(t))$: social component

Equations (1) and *(2)* are the main rules that PSO employ for the search process.

6. OPTIMISATION PROBLEM

Strength problem is a maximisation optimisation problem which depends on six main parameters, and the whole issue can be described as follow:

Consider $\vec{x} = [x_1 \quad x_2 \quad x_3 \quad x_4 \quad x_5 \quad x_6] = [d \quad a_x \quad a_y \quad E_m \quad F_{ft} \quad E_f]$

Maximise

$$f(\vec{x}) = f_{1t} = F_{ft}\left(v_f + \frac{E_m}{E_f}\right)(1 - v_f) \tag{5}$$

Subject to $v_f \leq 0.6$

$$F_{1t} \leq 2.5\ GPa$$

$$5 * 10^{-6} \leq d \leq 40 * 10^{-6}$$

$$50 * 10^{-6} \leq a_x \leq 100 * 10^{-6}$$

$$50 * 10^{-6} \leq a_y \leq 100 * 10^{-6}$$

$$2 * 10^{9} \leq E_m \leq 5 * 10^{9}$$

$$2 * 10^{9} \leq F_{ft} \leq 5 * 10^{9}$$

$$40 * 10^{9} \leq E_f \leq 80 * 10^{9}$$

The above mentioned constraints were chosen based on characteristics in *Table 2* and *Table 3* considering the minimum and maximum values in these tables. *Figure 4* shows the performance of PSO on this constrained optimisation problem where it is required to find the best possible set of variables that can meet the requirement of the constraints. It is worth to mention that for the set of variables in *Table 3*, the corresponding maximum F_{ft} is 2.8241e + 09 while v_f is 0.5027.

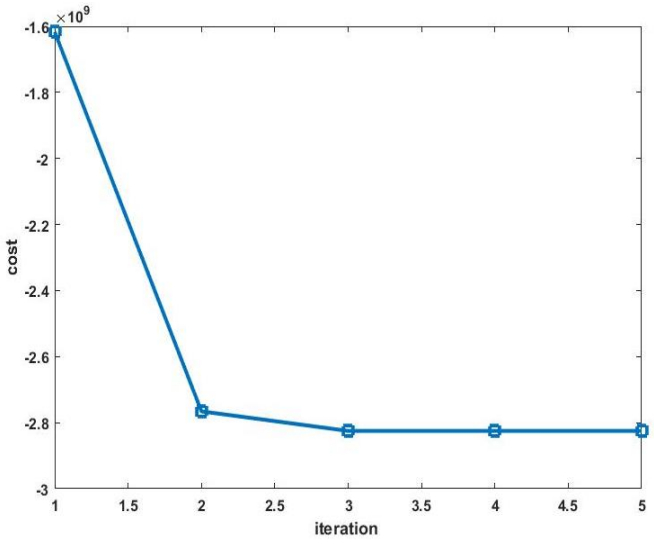

Figure 4. The convergence of the PSO on maximum strength equation

Table 4
Best possible results for the constrained problem

Parameter	***d mm***	***ax mm***	***ay mm***	***Em Gpa***	***Fft Gpa***	***Ef Gpa***
Value	4.0e-05	5.0e-05	5.0e-05	5	5	40

7. CONCLUSION

Design of composite material based on micromechanical analysis was adapted. Micro-mechanical analysis evaluates the characteristics of heterogeneous composite layer by representing it as homogeneous – anisotropic material. The analysis estimates the overall properties of the composite depending on other known (by tests) characteristics of the material. So it determines the strength and stiffness of the composite with in the fiber, matrix, and the interface. Micromechanical analysis is done under assumptions such as that the fibres are distributed periodically, the fibres are infinitely long, and each layer of the materials has homogeneity of orthotropic properties. Square RVE (unit cell) was adapted in this work.
Optimum design of Glass fibre-Epoxy composite material has been conducted through this study. Particle swarm optimisation was used to find the best design parameters including spatial elements of the unit cell as well as a given set of strength values for both Glass-fibre and Epoxy. For this problem, under given constraints, PSO was efficient enough to find the best possible design parameters within only five iterations.

The longitudinal tensile strength was optimally calculated considering the constraints of the problem such as the fiber volume fraction which was found as 0.5027 as optimum. From that, optimum diameter of fiber and the dimensions of the square unit cell were also found based on *Equation (2)*.

As a future work, there will be a comparison between the diameter influence on the design characteristics of the square unit cell and the hexagonal unit cell.

ACKNOWLEDGEMENTS

The described article was carried out as part of the EFOP-3.6.1-16-2016-00011 *Younger and Renewing University – Innovative Knowledge City – institutional development of the University of Miskolc aiming at intelligent specialisation* project implemented in the framework of the Szechenyi 2020 program. The realization of this project is supported by the European Union, co-financed by the European Social Fund.

REFERENCES

[1] Pimenta, S.– Pinho, S. T.: An analytical model for the translaminar fracture toughness of fibre composites with stochastic quasi-fractal fracture surfaces. *Journal of the Mechanics and Physics of Solids*, 2014, 66, pp. 78–102.

[2] Ramsteiner, F.–Theysohn, R.: The influence of fibre diameter on the tensile behaviour of short-glass-fibre reinforced polymers. *Composites Science and Technology*, 1985, 24 (3), pp. 231–240.

[3] Çuvalci, H.–Erbay, K.–İpek, H.: Investigation of the effect of glass fiber content on the mechanical properties of cast polyamide. *Arabian Journal for Science and Engineering*, 2014, 39 (12), pp. 9049–9056.

[4] Landesmann, A.–Seruti, C. A.–Batista, E. d. M.: Mechanical Properties of Glass Fiber Reinforced Polymers Members for Structural Applications. *Materials Research*, 2015, 18 (6), pp. 1372–1383.

[5] Alsarayefi, S.–Jalics, K.: The change of the NVH characteristics of composite vehicle components as a result of visible and not visible damages. In *Advances and Trends in Engineering Sciences and Technologies III: Proceedings of the 3rd International Conference on Engineering Sciences and Technologies (ESaT 2018), September 12–14, 2018, High Tatras Mountains, Tatranské Matliare, Slovak Re-public*. 2019. CRC Press.

[6] Kim, J.-W.–Kim, H.-S.–Lee, D.-G.: Tensile Strength of Glass Fiber-reinforced Plastic by Fiber Orientation and Fiber Content Variations. In *International Journal of Modern Physics: Conference Series*. 2012. World Scientific.

[7] Karas, L.–Jalics, K.–Priebsch, H. H.: Vibro-Acoustic Simulation of Aluminium Foam Parts Using MultiScale Techniques. *Advanced Engineering Materials*, 2011, 13 (11), pp. 1015–1018.

[8] Drugan, W.–Willis, J.: A micromechanics-based nonlocal constitutive equation and estimates of representative volume element size for elastic composites. *Journal of the Mechanics and Physics of Solids*, 1996, 44 (4), pp. 497–524.

[9] Mori, T.–Tanaka, K.: Average stress in matrix and average elastic energy of materials with misfitting inclusions. *Acta Metallurgica*, 1973, 21 (5), pp. 571–574.

[10] Eshelby, J. D.: The determination of the elastic field of an ellipsoidal inclusion, and related problems. *Proceedings of the Royal Society of London. Series A. Mathematical and Physical Sciences*, 1957, 241 (1226), pp. 376–396.

[11] Hossein Moini, P. o. M. E.: *Composite Materials*. [Lecture Notes] 2013, Available from: https://www.linkedin.com/in/hossein-moini-53188627/.

[12] Ghafil, H.–Jármai, K.: Comparative study of particle swarm optimization and artificial bee colony algorithms. In *Multiscience XXXII. MicroCAD International Multidisciplinary Scientific Conference*. 2018, Miskolc-Egyetemváros, Hungary.

Design of Machines and Structures, Vol. 9, No. 1 (2019), pp. 13–23.
DOI: 10.32972.dms.2019.002

INVESTIGATION AND OPTIMIZATION OF THE ACOUSTIC PERFORMANCE OF FORMULA STUDENT RACE CAR INTAKE SYSTEM USING COUPLED MODELLING TECHNIQUES

BARHM MOHAMAD[1]–KAROLY JALICS [2]–ANDREI ZELENTSOV[3]

[1, 2] University of Miskolc, Department of Machine and Product Design
3515 Miskolc-Egyetemváros, pywand@gmail.com
[3] Bauman Moscow State Technical University, Piston Engine Department,
105005 Moscow, Russia

Abstract: The University of Miskolc has previously designed and prototyped several race cars for the Formula Student (FS) competition. Unfortunately, none of these cars utilized air intake systems meeting all the requirements of regulations. Intake system are used to feed the engine with sufficient amount of air for complete combustion inside the combustion chamber to produce maximum power. The air flow during flowing produce sound waves due to rate of turbulence and boundary layer separation, and according to standard regulation this sound should be controlled minimum as possible. Recent advances in modelling procedures for accurate performance prediction have led to the development of modelling methods for practical intake system components in commercial design. Engine designers need simple and fast modelling tools, especially in the preliminary design evaluation stages. In this study, commercial software Solidworks and advanced design software Creo 4.0 were used in addition for that Computational Fluid Dynamics (CFD) analysis is performed. Frequency domain analysis is made to receive behaviour of the entire system under assumed conditions.

Keywords: *Intake system, sound pressure level, flow modelling, pressure drop, computational fluid dynamics, optimization*

1. INTRODUCTION

The air intake system is a major component required by internal combustion engines (ICE), and is critical regarding of the produced power of the ICE. However, in the investigated Formula Student (FS) car engine the current air intake system that was originally designed for it cannot used further due to significant power loss in certain engine speed ranges. The air intake system had seen many iterations of improvements, allowing the engine to produce increasing amount of power. This study takes a look at on the design process of the air intake system of the Formula Student [FS] car. Over the years, much of the design of this system had been carried out through an iterative trial and-error process, so the study attempts to identify the scientific and engineering principles pertaining to the design of this system. The intake system is being sub-divided into various components like restrictor, plenum and runner, then the relevant principles will be discussed. Following that, data is collected from the engine cylinders, cam-profile, intake valves etc. and a 1D simulation model of the engine will be developed using AVL Boost software. This model is then being applied *(Figure 2)*, sequentially, to the various components. Flow analysis for individual components are carried out and verified against performance simulations of the entire engine system, followed by physical testing data of several of the components from an authorised manufacturer dealer and University of Miskolc's engine test bed.

Computational Fluid Dynamics tools were used in this research work, such as AVL Fire software, aid the design process through virtual simulations, including data acquisition and analysis of design variations for better information on the effects without cycling through the manufacturing and assembly processes.

Other tools, including test rigs, such as a dynamometer, are used for physical testing of manufactured components of the air intake system with a running engine, and aid the designer in the validation of his design, which, when compared against calculations and simulations results, provides the confidence that the system is able to perform its designated task, to the required levels of performance. The engines used in the FS car competition are primarily piston-type reciprocating engines, and while the competition is dominated by race cars sporting inline-4-cylinder engines, the team has been using a Honda CBR 600RR (PC 37) engine for the last two years, particularly for its advantage in power-to-weight ratio.

2. MATHEMATICAL ANALYSIS

2.1. General

The intake system is made up of a few components placed in series and lie between the atmospheric air (intake orifice) and the intake valves of the engine. The primary function of the air intake system is to deliver air to the engine. It would be important to calculate the amount of air charge that can be sucked into the cylinder, as a ratio of the theoretical mass of air that can be contained in the cylinder. Essentially, for a naturally aspirated gasoline engine, it is the ratio of the trapped volume of gas to the volume of the cylinder (Claywell et al. 2006).

$$\lambda_a = \frac{m_g}{m_{th}} = \frac{m_g}{v_H \rho_{th}} = \frac{v_g}{v_H} \tag{1}$$

λ_a: Volumetric Efficiency;
$m_g = v_g \rho_g$: mass of air that is trapped in cylinder;
m_{th} = Theoretical mas of air that can be traaped in cylinder;
$v_H = v_{th}$ is Volume of Cylinder, which equals theoretical Volume;
$\rho_{th}\ or\ \rho_g$: Theoretical density of air in cylinder;
v_g: Volume of gas trapped in cylinder.

The method of charging the engine is by the depression (partial vacuum) created by the expanding of the combustion chamber due to the downwards moving piston. Theoretically it is possible to achieve a maximum volumetric efficiency of 100%. This value could be reduced by intake components start from restricted flow through the throttle body and intake valves, the energy loss through friction with the inner walls of the air intake system, as well as the propagation of reduced air pressure when the cylinder's vacuum initiates. The mass flow rate under a choked flow condition can be defined by the *Equation (2)*:

$$\dot{\boldsymbol{m}} = \boldsymbol{C_D A_c} \sqrt{\boldsymbol{K \rho p} \left(\frac{2}{k+1}\right)^{\frac{(K+1)}{(K-1)}}} \tag{2}$$

$\dot{\boldsymbol{m}}$: Mass flowrate kg/s;
C_D: Discharge coefficient;
A_C: Discharge hole cross-sectional area, m^2;
$k = \frac{c_p}{c_v}$ = of the gas;
C_p: Specific heat of the gas at constant pressure;

C_v: Specific heat of the gas at constant volume;
$\boldsymbol{\rho}$: Real gas density at P and T in kg/m^3;
p: Absolute upstream pressure of gas, Pa.

The discharge coefficient is the ratio of the actual flow rate to the ideal flow rate of the gas, therefore in this calculation, a discharge coefficient of 1 is taken. See *Table 1* below:

Table 1
Gas and restrictor characteristics

Parameters	**Value**
Discharge coefficient C_D	1
Discharge hole cross-sectional area, m^2 (20 mm diameter restrictor)	3.142×10^{-4}
Specific heat of the gas at constant pressure J/Mol.K	29.19
Specific heat of the gas at constant volume J/Mol.K	20.85
Real gas density at p and T in kg/m^3	1.2041
Absolute upstream pressure of gas, Pa	101,325
Volume flowrate $\dot{v}$ m^3/s	0.0624
Mass flowrate $\dot{m}$ kg/s	0.075

In addition to the restrictions on the engine, that the engine must operate with gasoline, it must have an air intake restrictor through which all of the air entering the engine have to pass. On the intake manifold system, the restrictor has to be placed between the throttle mechanism and the engine itself. It also must not be movable or flexible in any way (Barhm 2017). This restrictor has to be circular in shape and limited to 20 mm in diameter. The dominant design of the FS race car has the engine located in the rear of the vehicle, driving non-steerable rear wheels (Baym 2006). From the specifications shown in *Table 2* below, the apparent reasons for using the Honda CBR 600RR (PC 37) becomes clear, with a higher power-to-weight ratio, the Honda CBR 600RR (PC 37) engine would be a preferred choice of engine.

Table 2
The specification of the base engine

Powertrain	Units					
Manufacturer / Model		Honda CBR600 RR (PC37)				
Cylinders & Fuel		Cylinders:	4	Fuel Type:	RON98	
Displacement & Compression		Displacement (cc):	599	Compression (_:1):	12.2:1	
Bore & Stroke	mm	Bore:	67	Stroke:	42.50	
Connecting Rods Length	mm	91				
Valve Train		Chain driven, DOHC				
Valve Diameters	mm	Intake	27.5	Exhaust	23	
Valve Timing	deg	Intake	Opens	at 1 mm lift	22° BTDC	
			Closes	at 1 mm lift	43° ABDC	
		Exhaust	Opens	at 1 mm lift	40° BBDC	
			Closes	at 1 mm lift	5° ATDC	
Firing Order		1-2-4-3				
Fuel Pressure	bar	4.00				

2.2. Intake runners

The intake runners are the parts of the air intake system which delivers air from the intake manifold to the cylinders *(*see *Figure 1)*. In each runner, the dominant phenomenon that governs its performance is actually the effect of acoustic waves. As the purpose of the runner is air delivery, its performance is pegged to how much air it can deliver, and the subsequent improvement of the volumetric efficiency (Guy 2006).

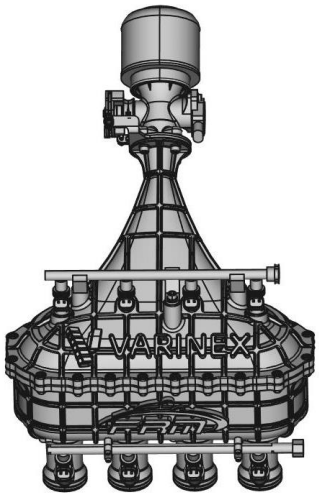

Figure 1. Intake system of FS car engine

2.3. Air ramming using tuned intake runners

The behaviour of acoustic waves in the runners resembles sound waves travelling through an open tube. An acoustic wave is a longitudinal wave made up of alternating regions of compressions and decompressions. In an intake runner, similar compressions and decompressions are occurring. The objective of a tuned intake runner would be to manipulate this reflected wave (while the engine is running at a desired engine speed) to make sure that a high-pressure region coincides with a subsequent valve opening. This is improving air-flow into the cylinder, improving the volumetric efficiency, hence achieving peak torque at the required engine speed (Vitek 2002). The source amplitude and impedance can be plugged upstream to the entire line to calculate the sound pressure level transmitted from the orifice as shown in *Figure 1*. The source reflection factor is related to the source impedance (Z) by *Equation 3*:

$$Z = \rho c \frac{1+r}{1-r} \tag{3}$$

Where (r) is reflection factor

For a real source from the engine, the reflection factor could be frequency dependent, since the source tends to be a velocity source at low frequencies and pressure source at higher frequencies.

2.4. Selecting a length for the intake runners

The calculation for the length of the tuned intake runners is based upon the duration between two events of the intake valve's operation: the first being the closing of the intake valve, and the second being the re-opening of the intake valve on the next cycle. The trade-off for using a shorter length runner is that as the acoustic waves propagate back and forth, they will constantly lose energy, so as the runner is designed to accommodate a higher order harmonic, and therefore designed to be shorter and easier to package on the FS car, it is also suffering the effects of a decreased ability to improve volumetric efficiency through the ramming effect of the acoustic waves.

3. COMPUTATIONAL TOOLS

AVL Powertrain software is a powerful and simplified that allows a user to quickly carry out a Computational Fluid Dynamics (CFD) analysis on a certain assembly. It comes with a user-friendly wizard that allows the user to set up the fluid flow and fluid forces analysis.

In this segment, the AVL Advanced Simulation software is used to analyze the airflow in the air intake system. It allows the user to check on the feasibility of the designed component and carry out an initial evaluation on the feasibility and quality of a certain design.

3.1. 1D configuration

In this section, the design of the Honda CBR 600RR (PC 37) engine is being scrutinized, including the collection of data for various components of the cylinders, and creating a working model for the engine, to simulate the four cycles of the engine for further computer simulations and analysis of the intake system.

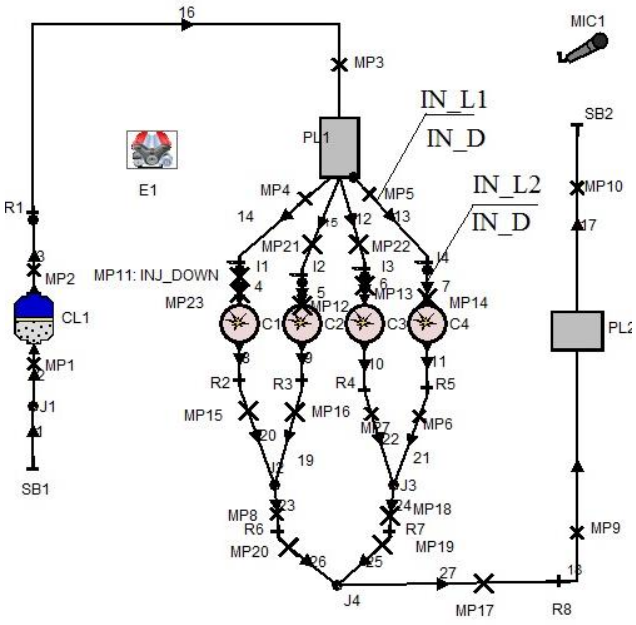

Figure 2. Engine scheme: modified parameters – volume of PL1, Intake ports length and diameter (IN_L1, IN_L2, IN_D)

3.2. 3D configuration

The optimization of the shape of the plenum is achieved in connection with CFD simulation (solver 3D Fire Advanced Flow) the intake manifold meshing process has been made for it with 3,115,552 elements with the geometrical optimization of the generic model of the plenum more detail of geometry shown in *Table 3*.

Table 3
Model properties

Type of model	3D
Type of mesh	Mapped
Total number of elements	3,115,552
Volume of model	0.004449 m^3
Surface area	0.346168 m^2

The basic method used is to refine the background mesh in the region of the surfaces defined in the STL file, then remove cells that are external to the flow path, and finally snap the vertices of the cells to the STL surfaces. Control of the mesh resolution is available at various points in the meshing see *Figure 3*. All obtained geometric parameters of the intake manifold and other part of engine from the 3D scan of the engine were entered into the 1D model (such as variable diameters of the intake and exhaust pipes dependent on their length, angles in the pipe joints of the intake and exhaust manifold, materials with thermal properties, etc.). Boundary condition were set according to the engine operation, and for the air flow through restrictor to the runner k-ζ-f model was set as turbulence model to treat the turbulence regime in the present study in the simulation, and nearly random fluctuations in velocity and pressure in both space and time.

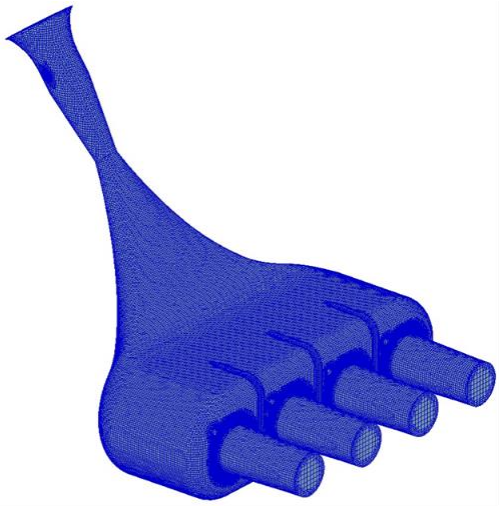

Figure 3. 3D inner volume of Honda CBR 600RR (PC 37) intake system, after applying mesh

4. RESULTS

From the results shown, the improved model is documented and illustrated as Mod 1 and Mod 2 then compared with base and Honda Manufacture Company data. One of the clearest features is that the intake runner diameter was increased in Mod 1 and the plenum volume was decreased 50%, significant effect was occurred on torque line *(*see *Figure 4)*. In Mod 2 the length of runner was increased from 100 to 250 mm, the diameter was reduced from 33.5 to 32 mm, and the PL1 (Plenum) volume was reduced from 4 to 3 litres.

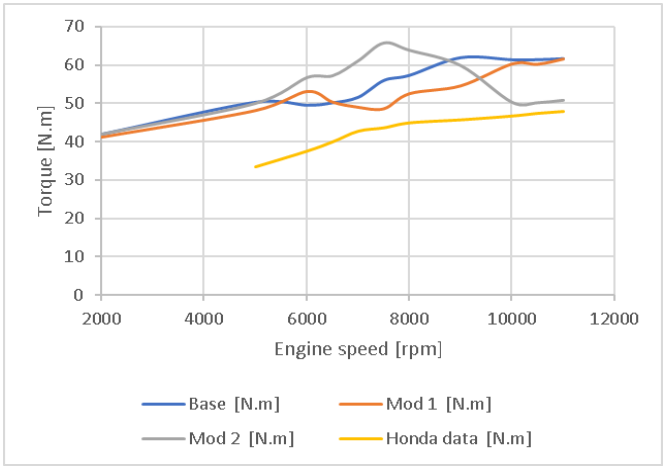

Figure 4. Comparison Torque from Honda data Co. with the base case, and two modifications 1, 2 from the software

The method here outlined may be adopted for both fluid dynamic and acoustic predictions, and then to evaluate the engine performance. The analytical of sound pressure level (SPL) solution of a simple plenum and was performed and optimized based on intake system geometry modification. Details in *Figure 5*.

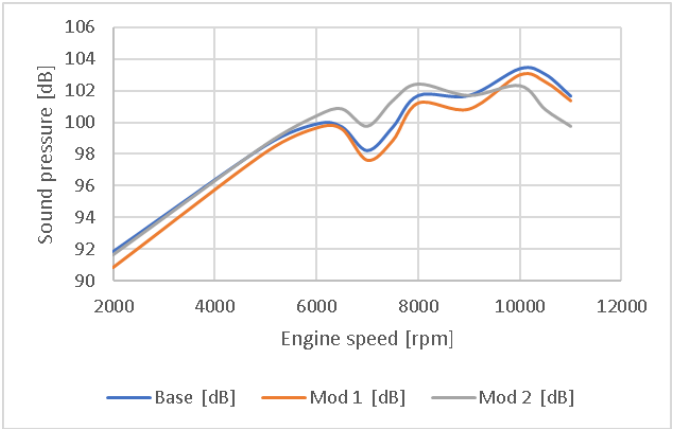

Figure 5. Comparison SPL between base case set and the modification 1 and 2

These design candidates were numerically implemented, and the results compared with results from base case set. In order to see the improvement through the design modification of intake system in case of rate of fuel consumption, Mod 1 and Mod 2 were also compared. It turned out, that the improvement Mod 1 has the minimum rate of fuel consumption as shown in *Figure 6*.

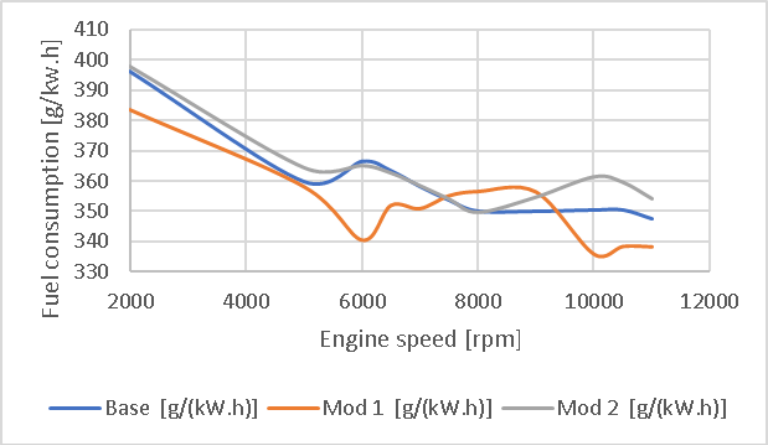

Figure 6. Comparison of the rate of fuel consumption of the base and modification 1, 2

3D CFD analysis was performed at various stages in the design. Simulation was used to evaluate two important flow properties which is velocity and pressure. The velocity logically high in plenum zone and runner part which may lead to fluctuation in amount of air into the combustion chamber at high engine speed *(Figure 7)*.

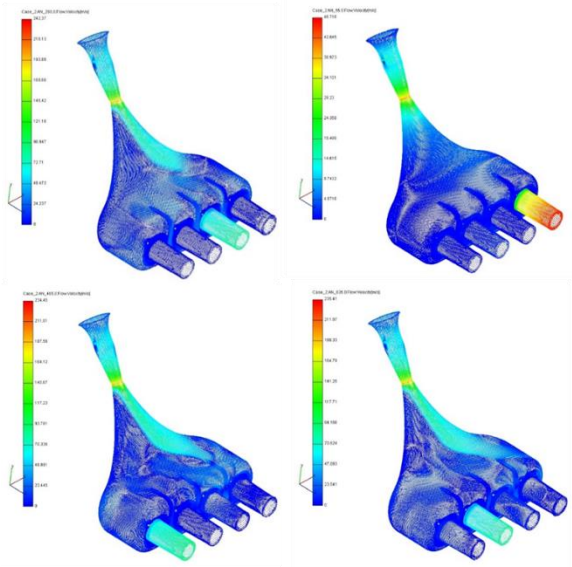

Figure 7. Velocity contour Min = 0, Max = 268.4 m/s at 8,000 rpm

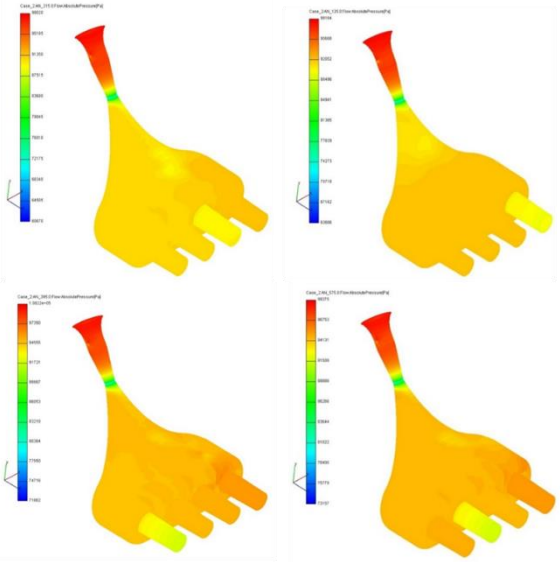

Figure 8. Pressure contour Min = 72217, Max = 1.00036e + 05 Pa at 8,000 rpm

The variations of diameter and length of runner from the current designs did not show strong effects on the overall heat release in compromised intake system.

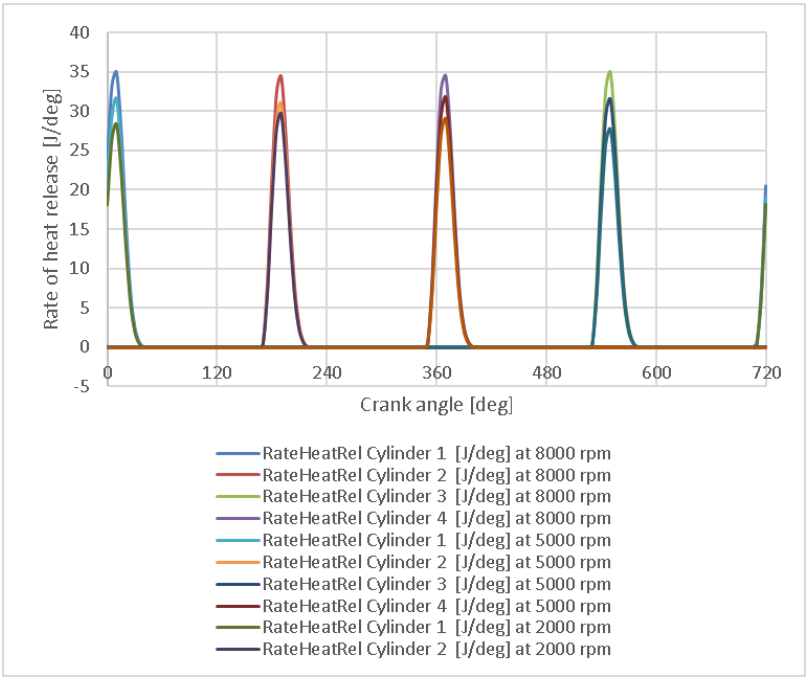

Figure 9. Rate of heat release in engine cylinders at 2,000, 5,000 and 8,000 rpm

5. CONCLUSION

The simulation was also carried out to explore the effect of the intake system geometry using a CFD perspective. The simulations were then carried out with flow being done in the three conditions: In comparison with the base case, in the modifications 1 and 2 the next parameters are modified:

- Mod 1 – the diameter of the inlet channel IN_D was increased from 33.5 to 42 mm (see engine scheme in *Figure 2*), as well as the volume of the intake manifold PL1 was decreased from 4 to 2 litres.
- Mod 2 – the length of inlet port IN_L1 was increased from 100 to 250 mm, IN_D diameter was reduced from 33.5 to 32 mm, PL1 volume was reduced from 4 to 3 litres.

The changes were carried out step-by-step search of options with different diameters, volumes and lengths, the optimality criterion was the effective performance of the engine at different operating modes (2,000–11,000 rpm). However, this optimization procedure was performed in manual mode (search of optimal sizes with the use of Case Sets), it was not done completely automatically using AVL Boost optimizer. The advantage of using coupled 1D/3D CFD simulations is to set reliable boundary condition for simulation and presenting accurate results.

The torque is given in results. Heat release rates are available only for cylinder units (in points MP 23, 12, 13, 14 there are data for the inlet, in points MP 15, 16, 7, 6 for exhaust). Overall, it had been a rewarding experience learning about the system and carrying out tests to delve deeper into the engineering and science behind it.

ACKNOWLEDGEMENTS

The described article was carried out as part of the EFOP-3.6.1-16-2016-00011 *Younger and Renewing University – Innovative Knowledge City – institutional development of the University of Miskolc aiming at intelligent specialisation* project implemented in the framework of the Szechenyi 2020 program. The realization of this project is supported by the European Union, co-financed by the European Social Fund.

REFERENCES

[1] Claywell, M.–Horkheimer, D.: Improvement of Intake Restrictor Performance for a Formula SAE Race Car through 1D & Coupled 1D/3D Analysis Methods. *SAE 2006 Motorsports Engineering Conference & Exposition*, December 2006, SAE 2006-01-3654.

[2] Barhm Mohamad–Gábor Szepesi–Betti Bollo: Combustion optimization in spark ignition engines. MultiScience – *XXXI. microCAD International Multidisciplinary Scientific Conference*, 2017, ISBN 978-963-358-132-2.

[3] Baym, B. et al.: An Experimental Approach to Design, Build, and Test a Throttle Body and Restrictor System for Formula SAE Racing. *SAE 2006 World Congress and Exhibition*, April 2006, SAE 2006-01-0748.

[4] Guy, R. et al.: Use of Computational Fluid Dynamics (CFD) Tools for High-Performance Engine Tuning. *SAE 2006 Motorsports Engineering Conference & Exposition*, December 2006, SAE 2006-01-3666.

[5] Vitek, O.–Polasek, M.: Tuned Manifold Systems – Application of 1-D Pipe Model. *Modeling of SI Engines and Multi-Dimensional Engine Modeling*, SAE 2002-01-0004.

[6] Barhm Mohamad–Gábor L. Szepesi–Betti Bollo: *Review Article: Effect of Ethanol-Gasoline Fuel Blends on the Exhaust Emissions and Characteristics of SI Engines*. Lecture Notes in Mechanical Engineering, 2018, ISBN 978-3-319-75677-6.

Design of Machines and Structures, Vol. 9, No. 1 (2019), pp. 24–28.
DOI: 10.32972.dms.2019.003

ANALYSIS OF THE DYNAMIC BEHAVIOR OF THE CNC MACHINE CENTER BY FEM

RÓBERT KISS–ATTILA SZILÁGYI

University of Miskolc, Department of Machine Tools
3515 Miskolc-Egyetemváros
robert.kiss9405@gmail.com, szilagyi.attila@uni-miskolc.hu

Abstract: This note is the first part of an extended research-analysis work, where our aim is to summarize the concepts of the methods and measurements, which we will present in the later articles. The research is focusing on the dynamic behavior of the DMU 40 5-axis CNC machine center, which can be found in the workshop of the Department of Machine Tools. This means that we would like to determine the magnitude of the dynamic stiffness of the machine tool, by calculating the value of the natural frequencies by final element method (analytically, and with software), and with the help of an experimental test.

Keywords: *natural frequency, DMU 40, FEM, analytical method, dynamic stiffness, ANSYS WB 19.1*

1. INTRODUCTION

The dynamic test was based on a 5-axis CNC machining center, which located in the department's workshop. The *Figure 1* is shown the machine tool catalogue picture, and the figure of the machine tool without paneling. We will perform the differential mechanical tests on the machine tool shown in this picture. The analysis may be performed by calculation or measurement, which are detailed in the followings.

Figure 1. DMU 40 CNC machine center catalogue image, and without paneling [1]

Basically, we can distinguish between three types of tests:

- Final element method in an analytical way,
- Final element method by software (ANSYS WB 19.1),
- The experimental determination of natural frequencies.

2. A BRIEF PRESENTATION OF EACH TYPE

In this chapter we present the fundamentals of the different types, on the basis of which we carry out the subsequent examinations. It is explained in more details later in the article.

2.1. Analytical method

Because of the complexity of the physical world, models need to be set up to describe the phenomena, embodying important properties for the analysis. The most important models in the mechanics like the rod, plate, point and rigid body models. In the mechanical vibration fields, more abstract models can be set than in other areas of mechanics. Establishing the motion equation system is the most difficult task in this process, after the setting up a vibration model. *Figure 2* shows the process of this method.

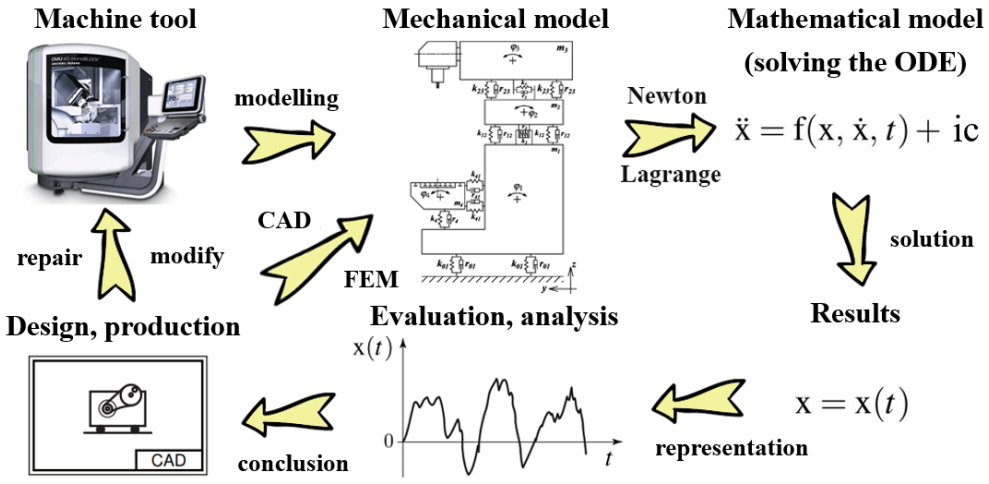

Figure 2. Process of engineering solutions for vibration problems [3]

The main steps of the process:

1. Establishing the mechanical model of the machine being tested.
2. Setting up the mathematical model based on the mechanical model (the motion equation is specified in the form of a differential equation system).
3. Solve the obtained motion equation with some mathematical method.
4. Plot the results with the help of diagrams, then analysis, evaluation.
5. Conclusions, modification of the machine or technical plan under examination based on the results of the examination.

During the analysis we can check the results obtained and the correctness of the mechanical model. Many of the unknowns in the FEM model make it difficult to track the effects of the parameters.

In the first phase of the product design, kinematic and dynamic analysis of the motion of each machine is essential. Even with simple models, the motion equation of the system is complicated. Typing and solving of the mathematical model with classical methods (Newton–Euler, or Lagrange equations) for systems with higher complexity is almost impossible. Therefore, in recent decades, multi-body procedures have spread to deal with such cases, as they are suitable for creating a computer code that automatically writes and solves motion equations for a particular machine system.

2.2. Final element method by software – ANSYS WB 19.1

One of the most commonly used finite element method (FEM) for solving mechatronic tasks is the structural analysis. Mechanical engineering refers to the examination of mechanical elements during structural analysis, which may be a part of a machine, a lathe or a whole vehicle. In the calculations, the unknown displacement is calculated primarily and the additional quantities, elongation, tension and reaction force, can be derived for instance.

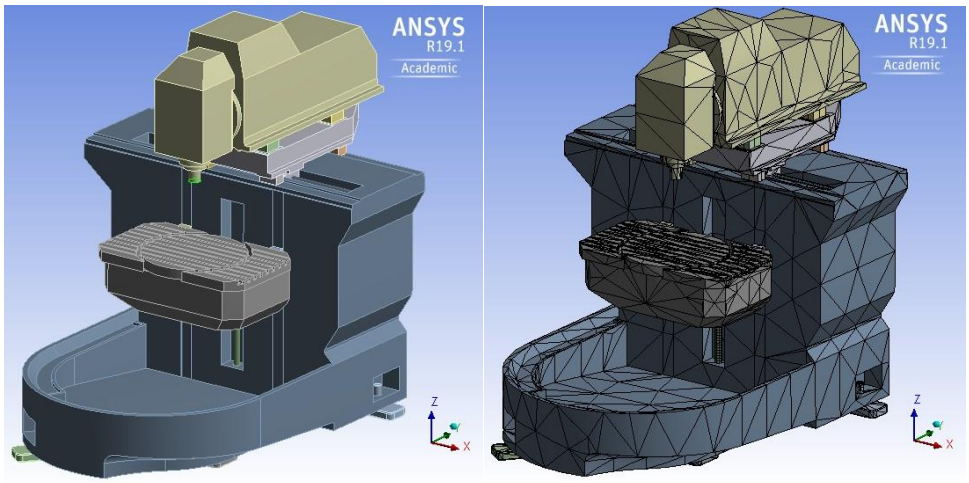

Figure 3. The 3D model in ANSYS

Possible types of the most important FEM analysis:

- Static analysis: It can be used to calculate permanent deformation or tension due to time-independent loading. However, the model may include time constant inertial loads (like angular velocity, or gravity), time varying effects (slow change of load) or time-dependent change of material (crawl).
- Modal analysis: It can be used to calculate the vibration characteristics of the test structure and to calculate the individual natural frequencies and to represent their oscillations, more detailed dynamic studies (e.g. transient dynamic, harmonic or spectral analysis) can serve as a basis.

- Harmonic response: It is used to determine a steady response to cyclically variable excitation in time. The analysis ignores transient phenomena the beginning of the load. It can predict the long-term dynamic behavior of the examined structure, examine the phenomenon of fatigue and resonance. The results of the test are summarized in the amplitude-frequency diagram.
- Spectrum analysis: An extended version of modal analysis. Determines the stress, response spectrum, or deformation given to the input of random vibration.

2.3. The experimental determination of natural frequencies

The determination of the frequencies of the different machines and equipment is important from several points of view, as the resulting error can be recognized in time and it can help to repair and re-design the equipment under examination, as well as to clarify the diagnosis established during the vibration test. On the basis of machine vibration, we can get a comprehensive idea of the machine state and the current state of each machine part.

In the field of vibration diagnostics, three typical test procedures have spread:

- bearing vibration test,
- resonance test,
- motion animation test.

In the future, we will deal with the resonance test, the other two types of which can be distinguished in practice by the applicability procedure. One type is the stop-ups analysis, which is the resonance frequency determination method for rotating machines, while the other is the external excitation study, which is used for machine tools, and applicable to motor vehicles. *Figure 4* shows the compilation of the above-mentioned external excitation study, which will be described in detail later.

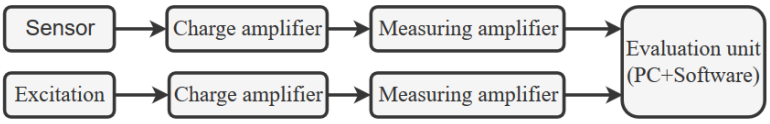

Figure 4. Sketch of a measurement assembly

3. SUMMARY

Based on the methods described above, various tests can be performed to determine the dynamic stiffness of the selected machine tool. In order to achieve the most precise production and to achieve the best surface quality, it is necessary to avoid the operation of the machining center at its natural frequencies and in their surroundings during machining.

ACKNOWLEDGEMENT

The described article/presentation/study was carried out as part of the EFOP-3.6.1-16-2016-00011 *Younger and Renewing University – Innovative Knowledge City – institutional development of the University of Miskolc aiming at intelligent specialisation* project implemented in the framework of the Szechenyi 2020 program. The realization of this project is supported by the European Union, co-financed by the European Social Fund.

REFERENCES

[1] *DMU monoBLOCK Series catalogue*, https://www.dmg.com, downloaded: 2018. 01. 26.

[2] Kiss R.: *CNC megmunkáló központ dinamikai viselkedésének vizsgálata végeselem-módszerrel*. Diplomaterv, Miskolc, 2019.

[3] Csernák G.–Stépán G.: *A műszaki rezgéstan alapjai*. Egyetemi jegyzet, Budapest, BME, 2012.

[4] Dömötör F.: *Rezgésdiagnosztika*. I. Dunaújvárosi Főiskola, Dunaújváros, 2008.

[5] Pascal, M.: *Parallelization of Design and Simulation: Virtual Machine Tools in Real Product Development.* Doctoral Thesis, ETH Zürich, 2012.

Design of Machines and Structures, Vol. 9, No. 1 (2019), pp. 29–47.
DOI: 10.32972.dms.2019.004

COMPUTATIONAL FLUID DYNAMIC SIMULATION OF LAMINAR FLOW OVER A FLAT PLATE

MOHAMAD MEHI ALDDIN KLAZLY–GABRIELLA BOGNÁR

University of Miskolc, Department of Machine and Product Design
3515 Miskolc-Egyetemváros
machhkme@uni-miskolc.hu

Abstract: The aim of this work is to apply CFD simulation on airflow over a flat plate to study the problem of hydrodynamic and thermal boundary layer and to analyse the effect of the length of the plate. The simulation ANSYS Fluent R18.1 has been applied to solve the governing equations of the flow. The simulation results have been verified by comparing the numerical solution with the analytical solution. The effect of changing the length of the plate is investigated while the other quantities were considered constant such as the free stream velocity, density, viscosity and temperature. The result showed excellent agreement between the numerical solution and analytical solution with maximum error of less than 6.19%. It is obtained that as the plate length increases the maximum value of the velocity contour, the Nusselt number, the wall shear stress, the skin friction coefficient and drag coefficient decreases.

Keywords: *CFD, boundary layer, numerical method, skin friction coefficient, heat transfer coefficient*

1. INTRODUCTION

Simulations of fluid mechanics flow using Computational Fluid Dynamic (CFD) are the key to solve many problems in mechanical engineering application. It has been used to understand fluid flow behaviour, which is essential in designing and developing any engineering application. One of the most common problems is flow behaviour in the boundary layer. Our aim is to consider hydrodynamic and thermal boundary layer problems of incompressible flow over a horizontal flat plate. The solution of the 2D laminar boundary layer of an incompressible flow formed on a semi-infinite plate has been introduced by Blasius using the similarity solution in 1908 [1], then, in 1938, Howarth gave a new solution using the Runge–Kutta method for analysing the flow over the flat plate [2]. Other methods in 1994, Abu-Sitta investigated and established the existence of the solution [3]. Moreover, the finite difference methodology was employed to get the numerical solution of the Falkner-Skan equation by Asaithambi [4], [5], [6]. Recently, the Blasius equation has been studied by applying different types of numerical and analytical techniques, for example using Adomain Decomposition Method (ADM) [7], [8], [9], and using Homotopy Perturbation Method (HPM) [10], [11]. Our work is motivated by the desire to apply the CFD simulation of flow over a flat plate and to obtain the numerical solution for the velocity and temperature distribution and to analyse at the wall the effect of plate's length on different variables.

2. MATHEMATICAL FORMULAS

Let us consider the problem of a two-dimensional flow of steady, Newtonian and incompressible fluid. The gravity is neglected, and all the fluid properties are assumed to be constant. When fluid flows over the impermeable plate, a thin boundary layer will develop

near the plate surface because of the no-slip condition. The viscous effect on the flow inside this layer is very important and has to be studied well, while region outside this hydrodynamic layer can be treated as an inviscid flow.

Laminar boundary layer equations:

We consider the problem of hydrodynamic and thermal boundary layer over a flat plate in a stream of air at temperature $T_\infty = 300$ K far from the plate and moving with uniform velocity $U_\infty = 1.5\ \mathrm{m/s}$. The temperature of the plate is $T_w = 400$ K. The governing equations, continuity, momentum and energy equations can be written as follows:

$$\frac{\partial u}{\partial x} + \frac{\partial v}{\partial y} = 0, \tag{1}$$

$$u\frac{\partial u}{\partial x} + v\frac{\partial u}{\partial y} = \upsilon\frac{\partial^2 u}{\partial y^2}, \tag{2}$$

$$u\frac{\partial T}{\partial x} + v\frac{\partial T}{\partial y} = \alpha\frac{\partial^2 T}{\partial y^2}, \tag{3}$$

where:
u and v: components of the velocity in *x* and *y* directions, respectively,
U_∞: free stream velocity,
T_∞: temperature of free stream,
α: thermal diffusivity of the fluid,
υ: kinematic viscosity of the fluid.

The fluid flow *Equations (1)–(3)* are subjected to the boundary conditions as follows:

at the plate as: $y = 0, \quad u = 0, \quad v = 0, \quad T = T_w,$ (4)

and far from the plate as $y \to \infty$, $u = U_\infty, \quad T = T_\infty$. (5)

The system (1)–(3) can be solved using similarity method applying stream function $\psi = \sqrt{2\upsilon x U_\infty}\, f(\eta)$, where f is the non-dimensional stream function and $\eta = y\sqrt{\frac{U_\infty}{2\upsilon x}}$ is the similarity variable. Then system (1)–(2) can be transformed into the well-known Blasius equation with $u = \frac{\partial \psi}{\partial y}$ and $v = -\frac{\partial \psi}{\partial x}$.

$$f''' + ff' = 0, \tag{6}$$

with boundary conditions

$$f(0) = 0, \quad f'(0) = 0, \quad f'(\eta_\infty) = 1. \tag{7}$$

For the energy *Equation (3)*, the similarity transformation $\emptyset = \frac{T-T_\infty}{T_w-T_\infty}$ is used. Then the *Equation (3)* is written as

$$\frac{\alpha}{\upsilon}\emptyset'' + \emptyset' f = 0, \tag{8}$$

with boundary conditions

$$\emptyset(0) = 1, \qquad \emptyset(\eta_\infty) = 0.$$

Applying Pr = $\frac{\alpha}{\upsilon}$ we have from (8)

$$\emptyset'' + Pr\ \emptyset' f = 0$$

The temperature and velocity components with similarity function f and $\emptyset$ are as follows $T = \emptyset(T_w - T_\infty) + T_\infty, \quad u = U_\infty f'(\eta)$ and $v = \sqrt{\frac{\upsilon U_\infty}{2x}}(\eta f' - f)$.

The analytical solution for the skin friction coefficient (C_f), the average Nusselt number ($\bar{N}_L$), average convection heat transfer coefficient ($\bar{h}$) and local Nusselt number (Nu_x) can be given by the expressions below [12]:

$$C_f = \frac{0.664}{\sqrt{\mathrm{Re}_x}}, \tag{9}$$

$$\overline{\mathrm{Nu}}_L = 0.664\,\frac{\rho U_\infty L}{\mu}, \tag{10}$$

$$\bar{h} = \frac{\bar{N}_L k}{L}, \tag{11}$$

$$\mathrm{Nu}_x = 0.332\ \mathrm{Re}_x^{\frac{1}{2}}\ \mathrm{Pr}^{\frac{1}{3}}, \tag{12}$$

$$C_D = \frac{F_x}{\frac{1}{2}\rho U_\infty^2 L}, \tag{13}$$

$$\mathrm{Re} = \frac{\rho U_\infty L}{\mu}, \tag{14}$$

$$\mathrm{Pr} = \frac{\alpha}{\upsilon}. \tag{15}$$

where:
C_f: skin friction coefficient,
C_D: drag coefficient,
Re: Reynold's number for the plate,
Re_x: Reynold's number at distance *x*,

ρ: density of the fluid,
μ: dynamic viscosity of the fluid,
L: length of the plate,
$\bar{h}$: average convection heat transfer coefficient,
$\overline{\mathrm{Nu}}_L$: average Nusselt number,
Nu_x: local Nusselt number,
Pr: Prandtl number,
k: thermal conductivity of the fluid,
F_x: horizontal force acting on the plate.

3. COMPUTATIONAL FLUID DYNAMICS METHOD (CFD)

Computational fluid dynamics is used for solving and analysing fluid flow problems numerically. The procedure of applying the CFD as the follow:

3.1. Creating the geometry

The first step is to model the problem and to create the geometry. The geometry of the model has created using Design Modeler. The flow configuration is represented in *Figure 1*. The boundary BC is defined as surface wall, AD defined as symmetry, and the boundaries AB and CD are defined as inlet and outlet, respectively.

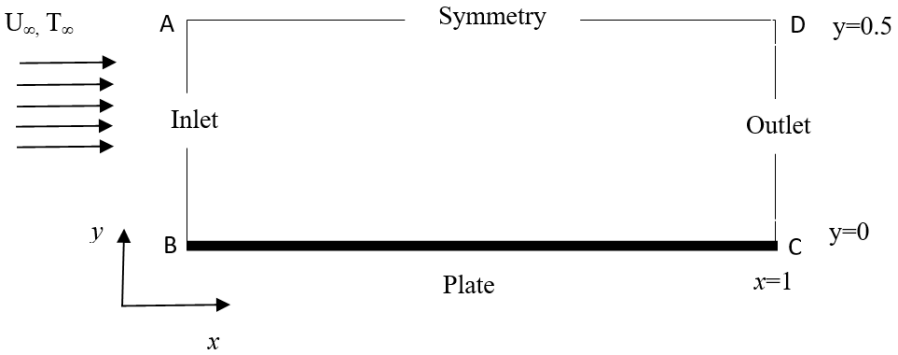

Figure 1. The flow configuration

3.2. Creating the mesh and name selection

Meshing is the second step of CFD simulation. For analysing the fluid flow, the flow domain splits into finer subdomains, for two-dimensional geometry it can be made up for quadrilaterals or triangles. Then, the governing equations are discretized and solved for these small subdomains. For our model the fluent mesh is used to create the meshing. The inlet and outlet have been divided by the number of division type with 100 divisions, the behaviour was set to hard with bias factor 100 to increase the number of subdomains near to the plate which is the important area and consequently the preciseness can increase. The sides symmetry and plate are divided using the same method with 60 divisions. *Figure 2* shows the result of mesh generation.

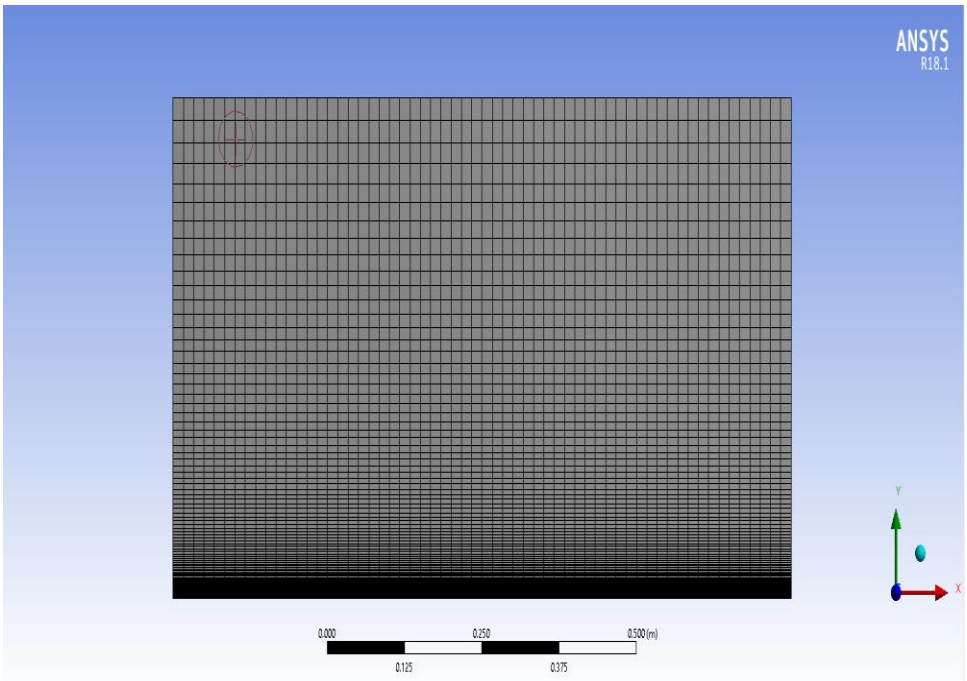

Figure 2. Meshing

3.3. Setting up the physical values

Here the flow and thermal variables (boundary conditions) on our physical model are specified. The boundary conditions and the fluid properties that have been used are the following according to the ANSYS FLUENT code. The boundary AB is defined as velocity inlet where the horizontal velocity is constant, and the vertical velocity is zero. The boundary CD is defined as pressure outlet, where the static pressure is placed equal to ambient pressure and all other flow quantities are extrapolated from the interior. The plate BC is defined as wall, where both the horizontal and vertical velocities are zero, and the far field AD is considered as symmetry where the velocity gradients in the vertical direction are forced to be zero. *Table 1* contains the physical properties of the fluid and flow.

Table 1
The physical properties

Name	Fluid properties	Value
density	ρ	1.225
dynamic viscosity	μ	1.7894×10^{-5}
length	L	1
ambient fluid velocity	U_∞	1.5
ambient fluid temperature	T_∞	300
wall temperature	T_w	400
thermal conductivity of the fluid	k	0.0242
Prandtl number	Pr	0.744176

3.4. Solution

The next step is to obtain the numerical solution, where the Navier–Stokes equations with the energy equation are solved. Laminar solver was used with second-order upwind scheme in the discretization of the set of governing equations. Double precision accuracy was used, and the solution was monitored using a residual monitor with convergence criteria 10^{-8}.

4. RESULT AND DISCUSSION

The results of the hydrodynamic and thermal boundary layers will be presented and discussed.

4.1. Hydrodynamic boundary layer

Figures 3 and *4* introduce the velocity distribution for the flow over the plate. The velocity at the plate is the lowest and it increases till became uniform in the inviscid area, which located above the boundary layer edge. The velocity vectors along with the plate *(*see *Figure 4)* shows that the velocity of fluid particles at the plate is zero due to the no-slip condition and this occurred due to the viscous effect, where the fluid particles stuck to the plate. The highest pressure was located near the leading edge and became lower as we go close to the outlet as can be seen in *Figure 5*.

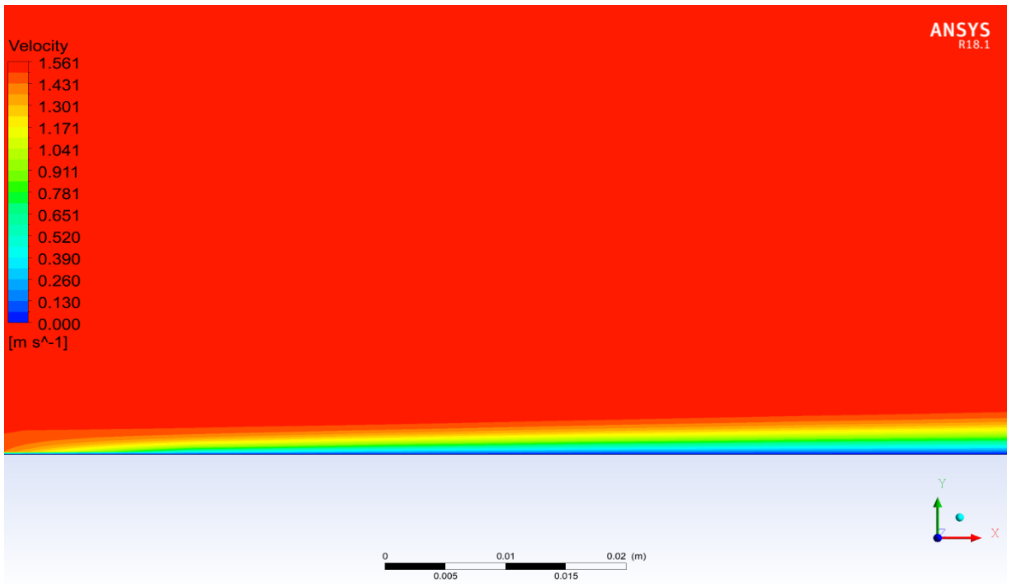

Figure 3. Velocity contour

Figures 6 and *7* show the comparison of velocities at three different locations at $\frac{X}{L} = \frac{1}{3}, \frac{X}{L} = \frac{2}{3}$ and $\frac{X}{L} = 1$. The maximum value of the velocity decrease from the left side to the right side far from the inlet, the maximum value of the velocity was 1.561 m/s *(*see *Figure 3)*.

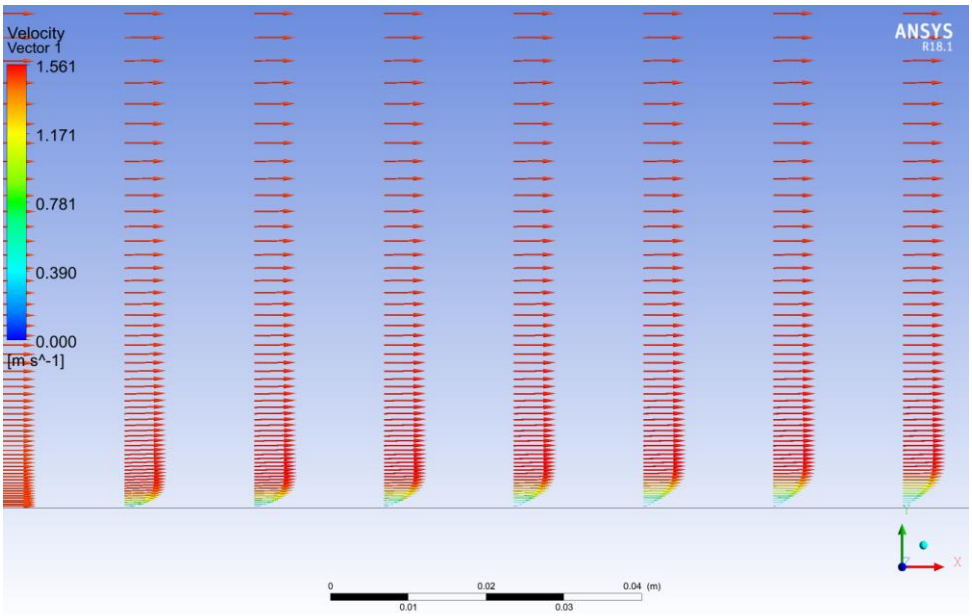

Figure 4. Velocity direction

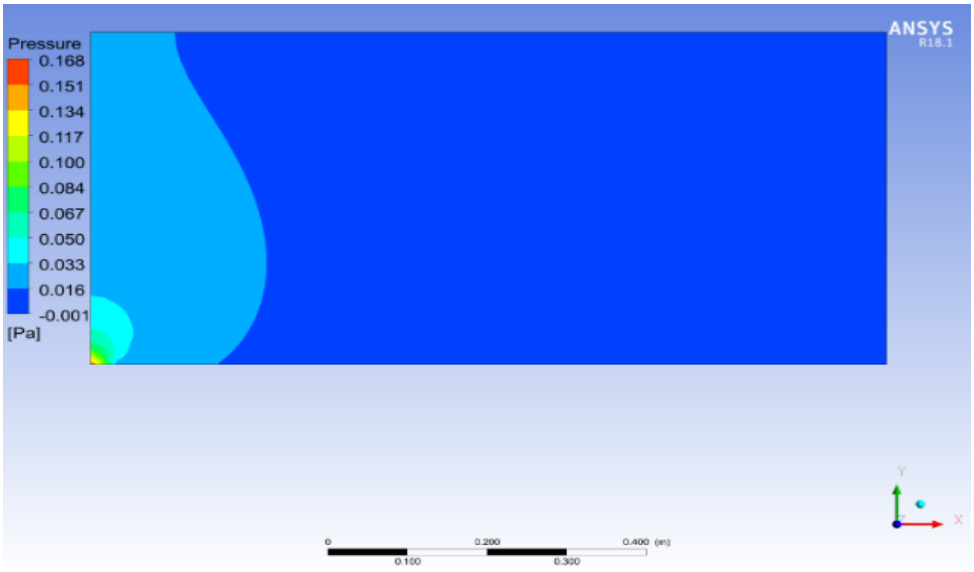

Figure 5. Pressure contour

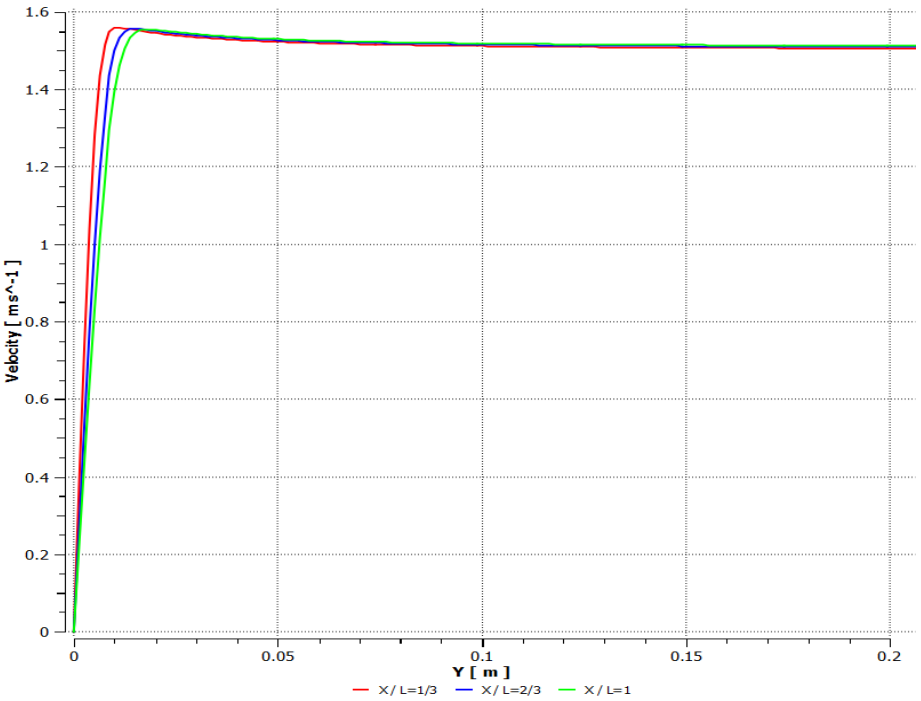

Figure 6. Velocity at different distances from the leading edge

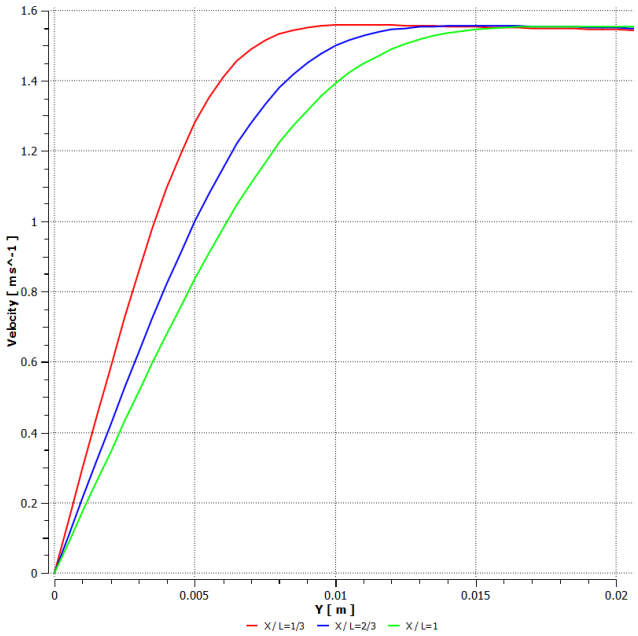

Figure 7. Velocity distributions at different distances from the leading edge

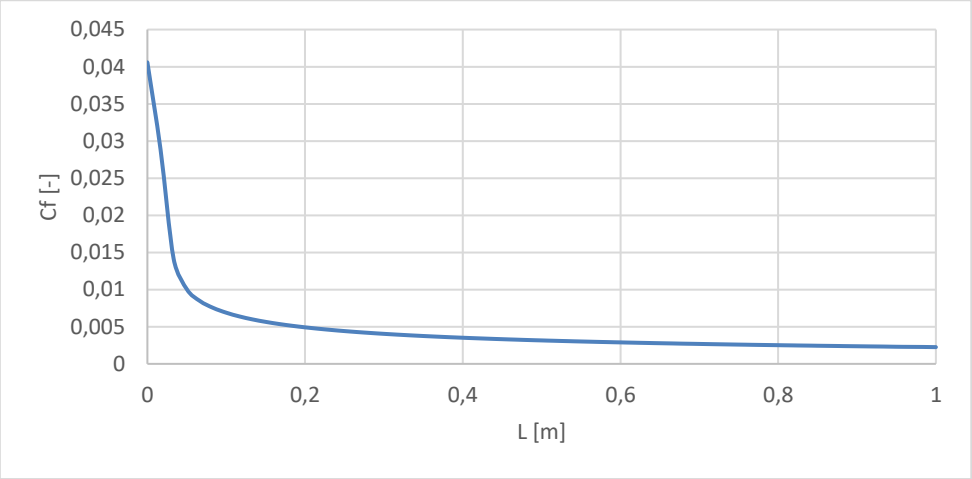

Figure 8. Skin friction coefficient

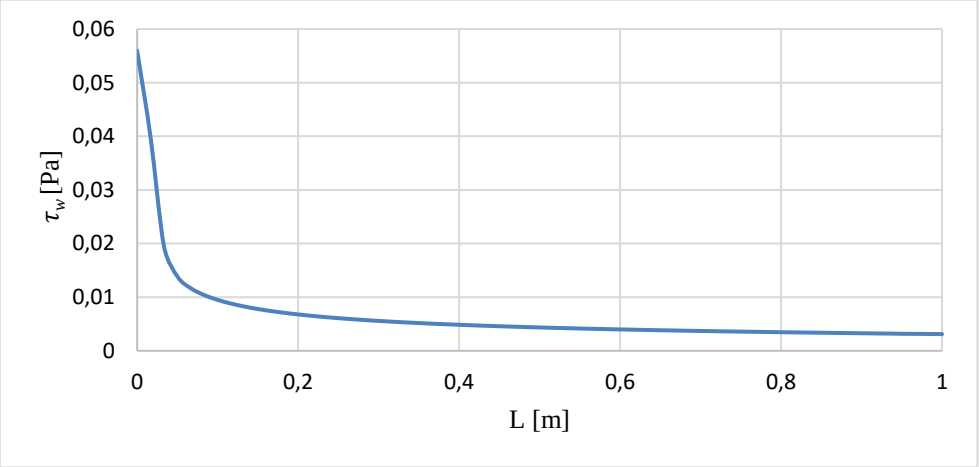

Figure 9. Wall shear stress

The skin friction coefficient is plotted on Fig. 8 along with the length of the plate, and value at the leading edge is 0.0405876 Pa. The wall shear stress is plotted on *Figure 9*. The value of shear stress at the leading edge of the plate was 0.0559349 Pa.

4.2. Thermal boundary layer

The result of the temperature distribution along the plate is presented in *Figure 10*. The temperature at the plate is the highest and it decreases till became uniform and equal to the free stream temperature which was 300 K. The variation of temperature due to the heat convention between the plate and the fluid mainly depends on the value of the thermal conductivity of the fluid.

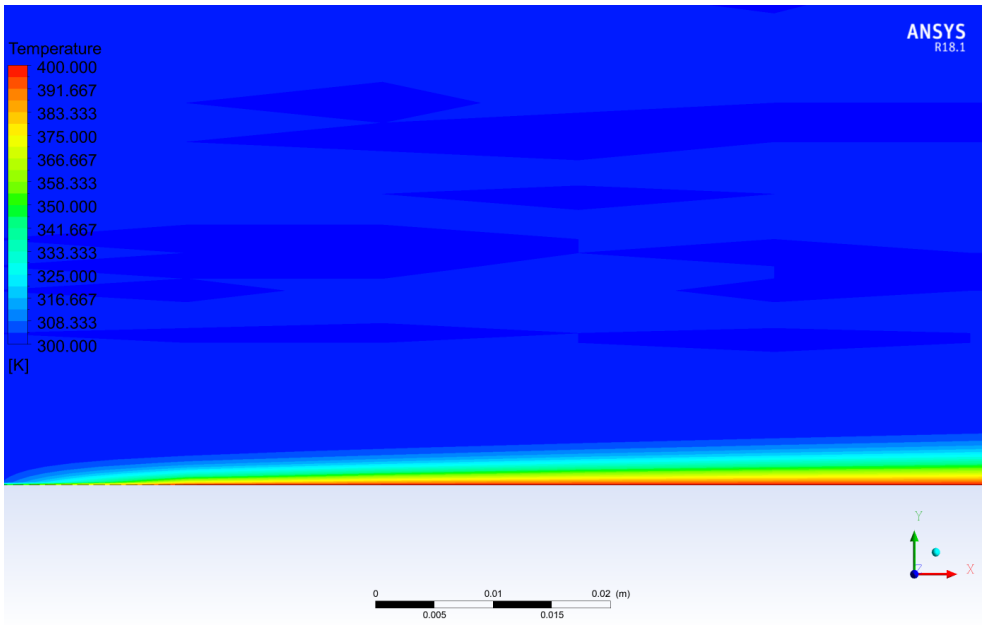

Figure 10. Temperature distribution

Figure 11 shows the total surface heat flux along with the plate and the surface heat transfer coefficient along the plate on *Figure 12*.

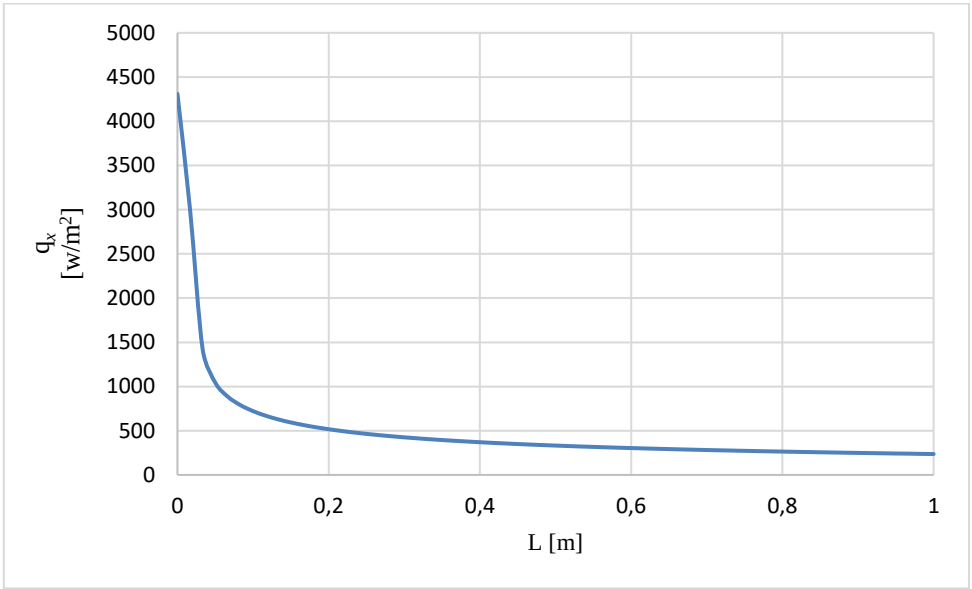

Figure 11. The surface heat flux along the plate

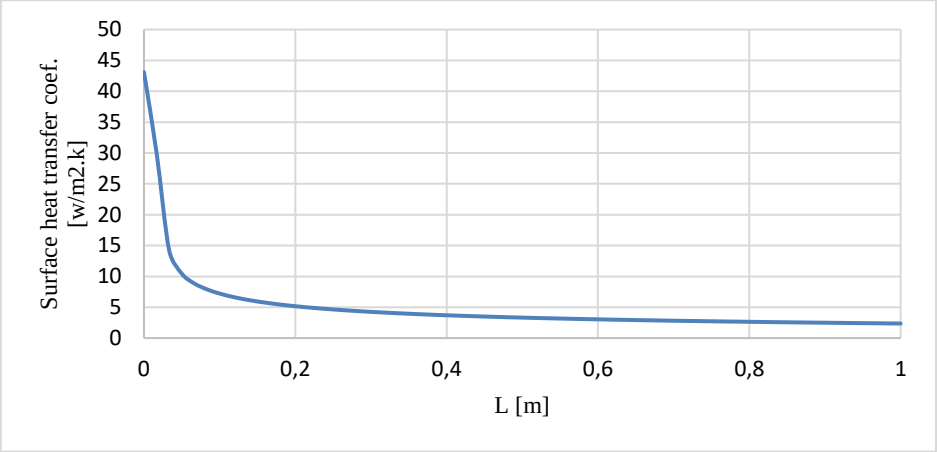

Figure 12. Surface heat transfer coefficient

5. VERIFICATION OF THE MODEL

The verification of the model has been done by comparing the CFD solution with the analytical solution of the average and local Nusselt number, average convection heat transfer coefficient, and the skin friction coefficient obtained via similarity technique [12] as the following:

5.1. Average Nusselt number ($\overline{Nu}_L$)

The comparison between the analytical and CFD for average Nusselt number ($\overline{Nu}_L$) shows good agreement and the error was only 2.896%. The result of the comparison presented in *Table 2* below:

Table 2
Result of ($\overline{Nu}_L$) CFD and analytical solution

Variable	Analytical	CFD	Error %
$\overline{Nu}_L$	192.820523	198.5766	2.896%

5.2. Local Nusselt number comparison (Nu_x)

The local Nusselt number can be calculated using the equation below:

$$Nu_x = \frac{q_x x}{(T_\infty - T_b)k}, \tag{16}$$

where:

q_x: heat flux at distance x,
x: distance from the leading edge,
T_∞: temperature of free stream,
T_b : bulk temperature of the fluid at x,
k: thermal conductivity of the fluid.

The local Nusselt number at different distances from the leading edge for the two solutions are shown in *Table 3*. The result shows a very good agreement between the two solutions. *Figure 13* shows the result of the comparison analytical and CFD solution of the local Nusselt number. The average error between the two solutions was 1.23%.

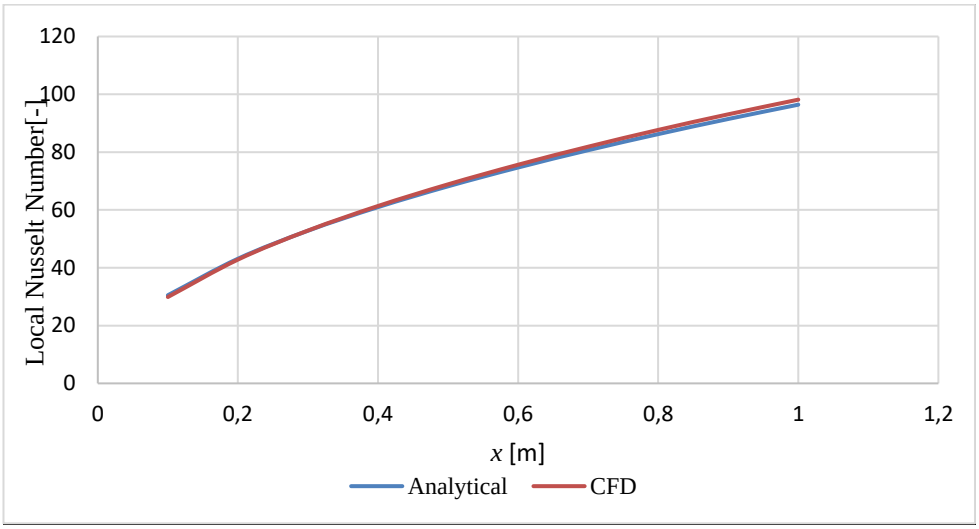

Figure 13. Comparison of analytical and CFD Results

Table 3
The result of local Nusselt Number

x	Analytical	Fluent	Error%
0.1	30.4876	29.8709	2.0645
0.2	43.1159	42.8180	0.6957
0.3	52.8060	52.8664	0.1141
0.4	60.9752	61.3597	0.6266
0.5	68.1723	68.8528	0.9882
0.6	74.6790	75.6342	1.2625
0.7	80.6626	81.8748	1.4795
0.8	86.2319	87.6792	1.6503
0.9	91.4628	93.0796	1.7363
1	96.4106	98.1585	1.7806

5.3. Average convection heat transfer ($\bar{h}$)

The results of $\bar{h}$, *Equation (8)* is presented in *Table 4* and it shows an excellent agreement between CFD and analytical solutions with only 0.0002% error.

Table 4
Result of comparison CFD and Analytical solutions

Variable	CFD	Analytical	Error %
$\bar{h}$	4.805554	4.66625	0.00002%

5.4. The skin friction coefficient

The skin friction using CFD is calculated by using the equation below:

$$C_f = \frac{0.664\tau_w}{\frac{1}{2}\rho\, v_b^2}, \tag{17}$$

where:
τ_w: wall shear stress at distance *x* from leading edge,
v_b: bulk velocity at distance x from leading edge,
C_f: skin friction coefficient,
ρ: density of the fluid.

A good agreement between CFD and the analytical solutions has been obtained. The results of the CFD and analytical solutions are represented in *Figure 14*. The average error between the two solutions is 6.19%. *Table 5* presents the results of the skin friction coefficient at a different distance from the leading edge. It shows that error is increasing with increasing value of *x*.

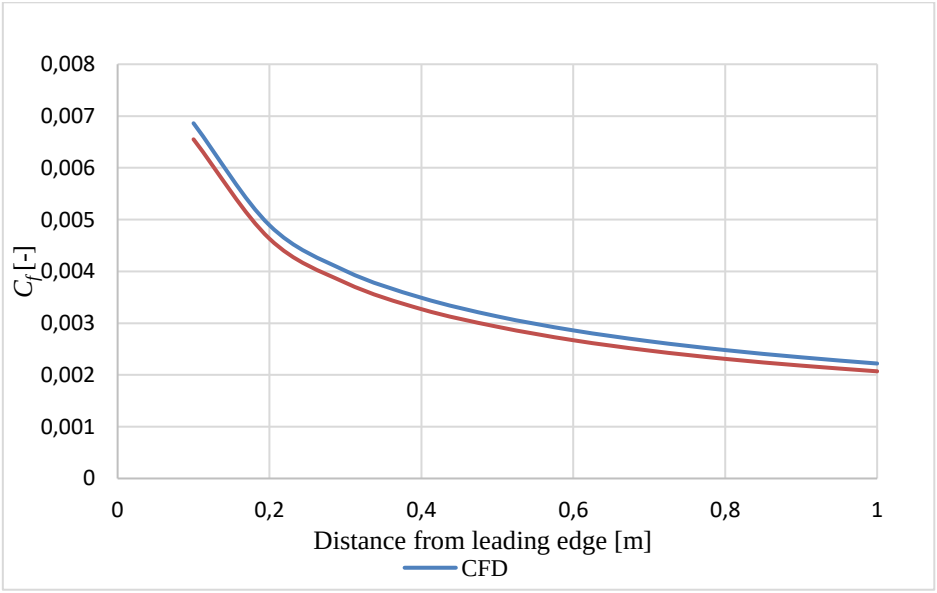

Figure 14. Comparison of the skin friction coefficients

Table 5
The skin friction coefficient

x	Analytical	CFD	Error%
0.1	0.00655	0.00686	4.49401
0.2	0.00463	0.00489	5.27362
0.3	0.00378	0.00401	5.78067
0.4	0.00327	0.00349	6.03457
0.5	0.00293	0.00313	6.37005
0.6	0.00267	0.00286	6.57521
0.7	0.00247	0.00265	6.74080
0.8	0.00231	0.00248	6.85560
0.9	0.00218	0.00234	6.87427
1	0.00207	0.00222	6.93961

6. ANALYZING THE EFFECT OF CHANGING THE LENGHT OF THE PLATE

Four simulations for different lengths from the leading edge was run for L = 0.8, 1, 1.2, and 1.4, with no change in the vertical dimension. All the model's properties in the model were fixed except the length of the horizontal dimensions. *Table 6* represents Reynolds' number for the four rectangles which were simulated for analysing the effect of changing the plate's length.

Table 6
Variation of the plate length

L	Re
0.8	82,150.44
1	102,688.05
1.2	123,225.66
1.4	143,763.27

6.1. The effect of the length on the velocity

The length of the plate effects on the velocity distribution and the boundary layer thickness. *Figure 15* shows the variation of the velocity at the outlet for different lengths. It is seen that the velocity decreases with the increment of the horizontal dimension and the boundary layer thickness gets higher values. The maximum value of the velocity was obtained for L = 0.8.

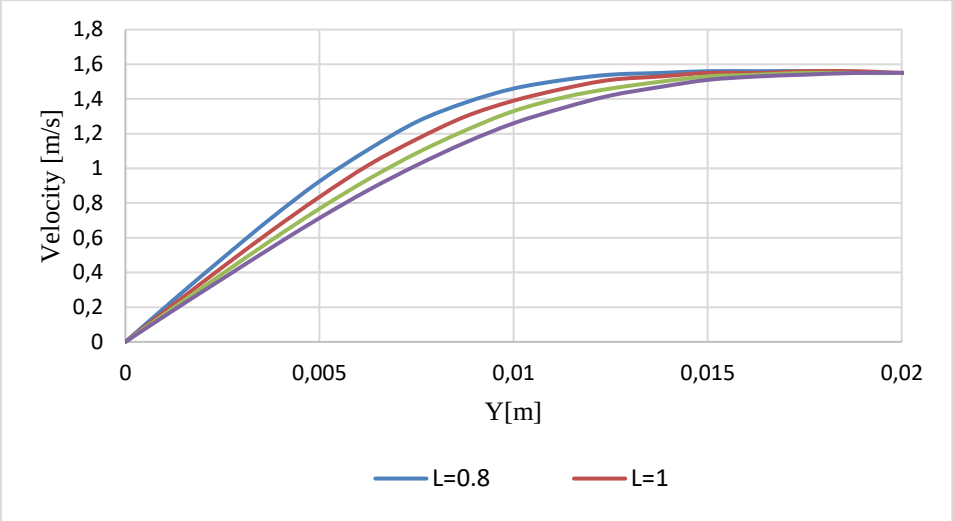

Figure 15. Velocity distribution and boundary layers for different plate's length

6.2. The effect of the plate length on the C_f, N_L, C_D, and τ_w

The skin friction coefficient plotted for the four length of the plate can be seen in *Figure 16* along with the length of the plate. At x = 0 the skin friction coefficient for L = 0.8 is 0.04517, for L = 1 is 0.04059, for L = 1.2 is 0.03715, and for L = 1.4 is 0.03446. The impact of the plate's length on the wall shear stress shown in *Figure 17* and *Table 7*, where the maximum value also was set as L = 0.8 and the wall shear stress is decreasing with increasing the plate's length. The comparison of the values of Nusselt number is plotted on *Figure 18*. It shows that the maximum value decreases with the increasing of the horizontal length. The conclusion is that the skin friction, wall shear stress and Nusselt number increase whenever the Reynolds number was increased. *Figure 19* demonstrates the variation of the drag coefficient with different plate lengths, it can be seen that the drag coefficient decreases as the plate length increases.

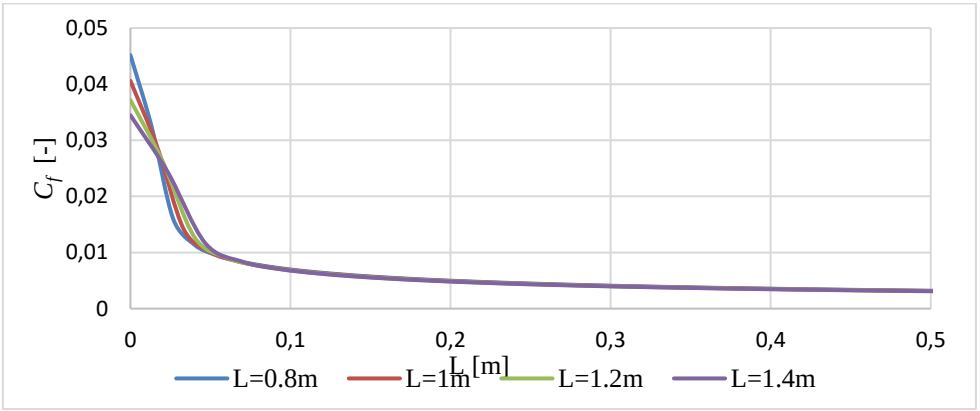

Figure 16. Skin friction coefficient for different plate's length

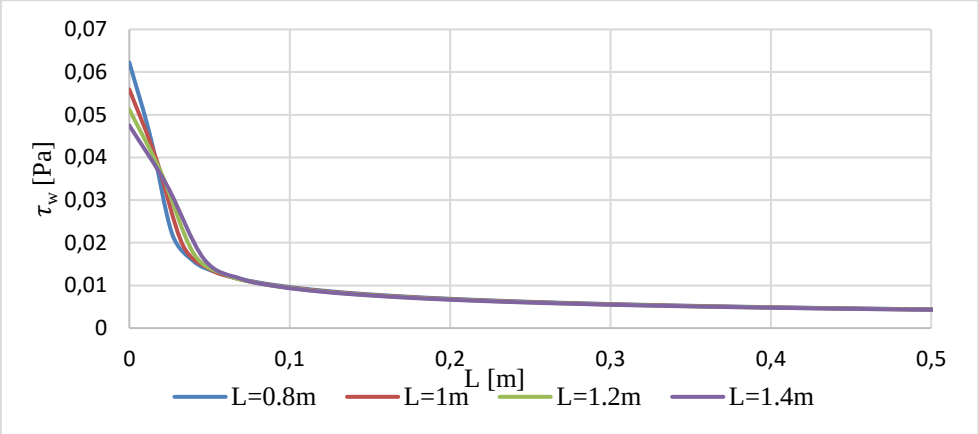

Figure 17. Wall shear stress for various L

Table 7
Wall shear stress at the leading edge

L	Wall shear
0.8	0.0622
1	0.0559
1.2	0.0512
1.4	0.0474

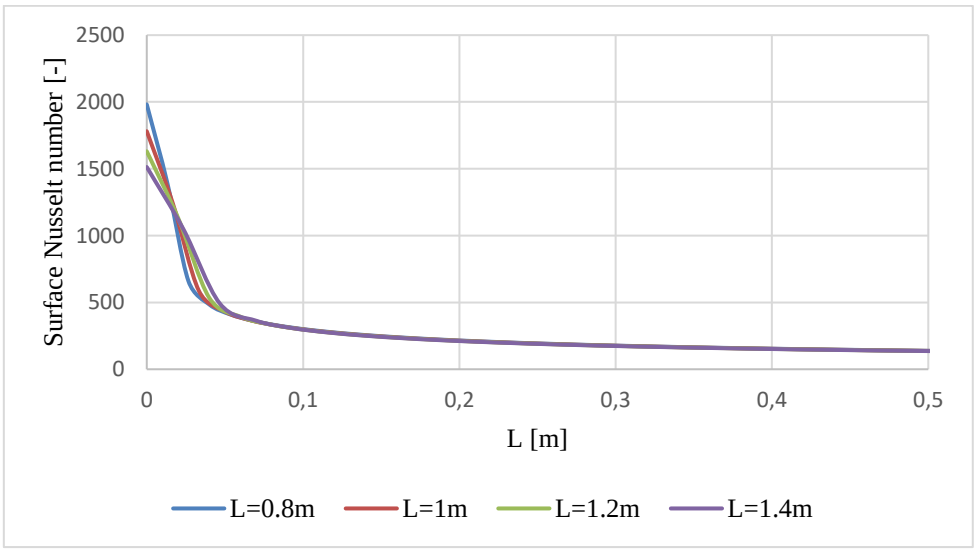

Figure 18. Nusselt number for different plate's lengths

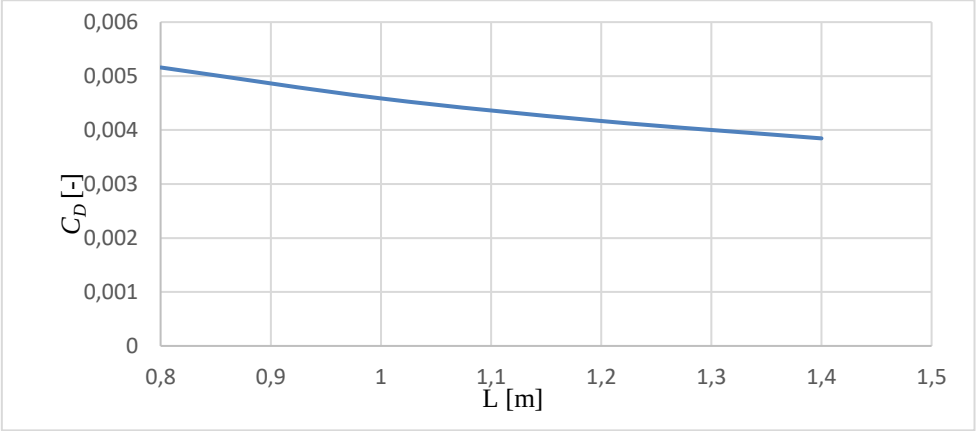

Figure 19. Drag coefficient for different plate's lengths

7. CONCLUSION

The hydrodynamic and thermal boundary layer of the air flow over a flat plate is numerically analysed using CFD simulation in two-dimensions. The results of the numerical and analytical solutions have been compared and showed good agreement for different variables in the model that have been simulated. Changing the length of the plate induced many effects on different dimensionless and dimensional variables such as Re, C_f, Nu, C_D, and the shear stress. Further study is recommended in the transition and turbulent flow for the same model.

NOMENCLATURE

C_f	–	skin frication coefficient
C_D	–	drag coefficient
F_x	N	horizontal force acting on the plate
$\bar{h}$	W/m^{2}k	average convection heat transfer
k	W/m.k	thermal conductivity of the fluid
N_{u_x}	–	local Nusselt number
$\overline{Nu}_L$	–	average Nusselt number
Pr	–	Prandtl number
q_x	W/m^2	heat flux at distance x
L	m	length of the plate
Re_x	–	Reynolds number at distance x
T_w	K	temperature of the plate
T_∞	K	temperature of free stream
T_b	K	bulk temperature of the fluid at x
u and v	m/s	components of the velocities
v_b	m/s	bulk velocity at distance x from leading edge

Greek symbols

υ	m^2/s	kinematic viscosity of the fluid
α	m^2/s	thermal diffusivity of the fluid

ρ	kg/m^3	density
μ	Pa/s	dynamic viscosity
τ_w	Pa	wall shear stress at distance *x* from leading edge.

Subscripts

w	wall
b	bulk

ACKNOWLEDGEMENT

The described study was carried out as part of the EFOP-3.6.1-16-2016-00011 *Younger and Renewing University – Innovative Knowledge City – institutional development of the University of Miskolc aiming at intelligent specialisation* project implemented in the framework of the Széchenyi 2020 program. The realization of this project is supported by the European Union, co-financed by the European Social Fund. The second author was supported by project no. 129257 implemented with the support provided from the National Research, Development and Innovation Fund of Hungary, financed under the K_18 funding scheme.

REFERENCES

[1] Blasius, H.: Grenzschichten in Flüssigkeiten mit kleiner Reibung. *Z. Math. Phys.*, 56 (1908), pp. 1–37.

[2] Howarth, L.: On the solution of the laminar boundary layer equations. *The Royal Soc. London*, A 164 (1938), pp. 547–579.

[3] Abu-Sitta, A. M. M.: A Note on a Certain Boundary-Layer. *Applied Mathematics and Computation*, 64 (1994), pp. 73–77.

[4] Zhang, J.–Chen, B.: An iterative method for solving the Falkner–Skan equation. *Appl. Math. Comput*., 210 (2009), pp. 215–222.

[5] Asaithambi, A.: Solution of the Falkner – Skan equation by recursive evaluation of Taylor coefficients. *Computational and Applied Mathematics*, 176 **(**2005), pp. 203–214.

[6] Bataller, R. C.: Numerical Comparisons of Blasius and Sakiadis Flows. *Matematika*, 26 **(**2010), pp. 187–196.

[7] Najafi, M.–Khoramishad, H.–Massah, H.–Moghimi, M.: A study of Blasius viscous flow : an ADM Analytical Solution. *Applied Mathematics*, 9 (2005), pp. 57–61.

[8] Wang, L.: A new algorithm for solving classical Blasius equation, *Applied Mathematics and Computation*, 157 **(**2004), pp. 1–9.

[9] Abbasbandy, S.: A numerical solution of Blasius equation by Adomian's decomposition method and comparison with homotopy perturbation method. *Chaos, Solitons and Fractals*, 31 (2007), pp. 257–260.

[10] Esmaeilpour, M.–Ganji, D. D.: Application of He's homotopy perturbation method to boundary layer flow and convection heat transfer over a flat plate. *Physics Letters*, A. 372 (2007), pp. 33–38.

[11] Ganji, D. D.–Babazadeh, H.–Noori, F.–Pirouz, M. M.–Janipour, M.: An Application of Homotopy Perturbation Method for Non-linear Blasius Equation to Boundary Layer Flow Over a Flat Plate Basic idea of homotopy perturbation method. *International Journal of Nonlinear Science*, 7 (2009), pp. 399–404.

[12] Schlichting, H.–Gersten, K.: *Boundary layer theory*. Springer Verlag, Berlin–Heidelberg–New York, 2000.

Design of Machines and Structures, Vol. 9, No. 1 (2019), pp. 48–53.
DOI: 10.32972.dms.2019.005

FINITE ELEMENT THERMAL SIMULATION OF A CNC MILLING MACHINE

TAMÁS KUNDRÁT–ATTILA SZILÁGYI

University of Miskolc, Machine Tools and Mechatronics Department
3515 Miskolc-Egyetemváros
kundrattamas@gmail.com
szilagyi.attila@uni-miskolc.hu

Abstract: This article concerns a thermal simulation of a 5-axis CNC milling machine by finite element method. At the early stage of a machine designing process, the analysis of thermal conditions is really important, because milling machines are exposed to heat effects. The result of it is a nonstationary temperature field, which can influence accuracy of positioning and it can generate thermal stress in the structure of machines. Besides harmful heat effects can decrease geometry accuracy of manufactured product, but making thermal analysis quality and lifecycle of products can be higher and planning time can be reduced.

Keywords: *thermal simulation, analysis, temperature field, accuracy, quality of product*

1. INTRODUCTION

Heat is appearance of energy in termodynamics, which occur between system and environment by difference of temperatures. In fact, heat sources in machine tools are energy sources which provide heat energy. Transfer of this energy can be realized by 3 different ways: conduction, convection and radiation. Conduction is vibration of molecules of material parts, convection is when atoms moves in macroscopic measure. Radiation is when electromagnetic radiation turns into heat energy.

2. DESCRIPTION OF TEMPERATURE FIELDS

In this section we detail the theory of temperature fields. Based on it, we can get information about distribution of temperature in machines. Generally temperature is a physical quantity as function of location coordinates as well as time coordinate

$$t = t(x, y, z, \tau). \tag{1}$$

Using this function, we can get temperature distribution over the domain realized by the investigated machine. As the result of time dependency, heat is treated as a transient problem. In that case when the time is fixed, the temperature field is stationary, hence the following functions are available

$$\begin{aligned} t &= t(x, y, z) \\ \frac{\partial t}{\partial \tau} &= 0. \end{aligned} \tag{2}$$

2.1. Specific transient curves of machine tools

At starting the machines heat generation begins from different heat sources on machines. During the process, the units continue heating and form a constantly changing temperature

field. By examining the equilibrium of heat quantities, it is possible to determine the warming curve, a temperature vs. time diagram that shows the way that the particular machine parts reach the constant temperature eventually. Practical warming curves may differ from the ideal, such as the starting grease-lubricated spindles shown in *Figure 1*.

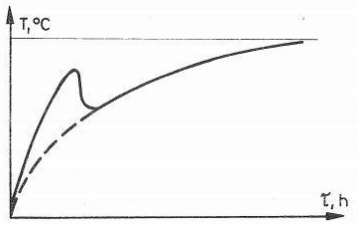

Figure 1. Ideal and practical warming curves [1]

3. SOLVING THERMAL PROBLEMS USING FEM (FINITE ELEMENT METHOD)

From a mathematical approach, the finite element method work with partial differential equations to solve engineering problems. We can use static, dynamic, vibration, thermal analysis and so on, and, besides, we can evaluate the simulation results and, moreover, product optimization is also possible. You can get information about faults during manufacturing process, and it is possible to draw up development directions. FEM is a complex way to analyse and solve thermal problems for example.

3.1. Thermal analysis of DMU40 milling machine

In this section the thermal analysis of a 5-axis CNC milling machine is presented. The investigation of the behaviour of a machine tool during milling process is performed. The 3D model of the machine tool is created first of all, then the influence of the milling tool, the workpiece, and several mechanical and thermal boundary conditions, like working temperature of bearing, cutting forces and temperatures, effect of cooling lubricant have been considered. Figure 2 shows the 3D model of analysed machine tool.

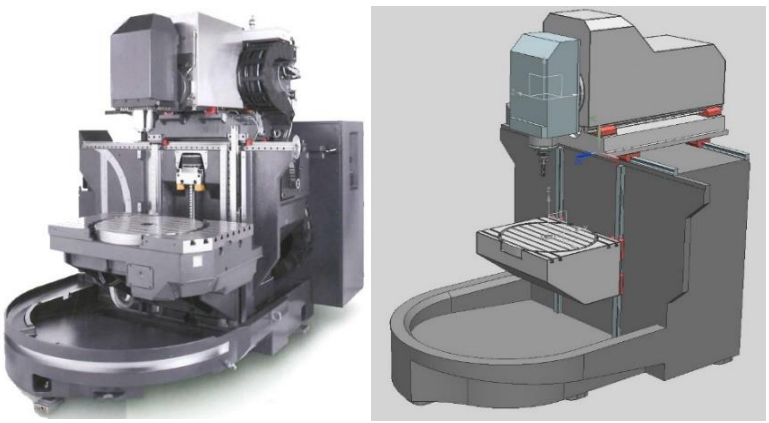

Figure 2. Result of the geometry modelling process – milling machine 3D model [2]

The analysed process is a primitive milling process using WIDIA Warimill 4777 tool with the following technological parameters. Diameter of tool is $D_1 = 20\ mm$, cutting speed is $v_c = 150 \frac{m}{\min}$ and the depths of milling are $a_p = 2\ mm; a_e = 10\ mm$. *Figure 3* shows the milling tool and sketch of the milling process.

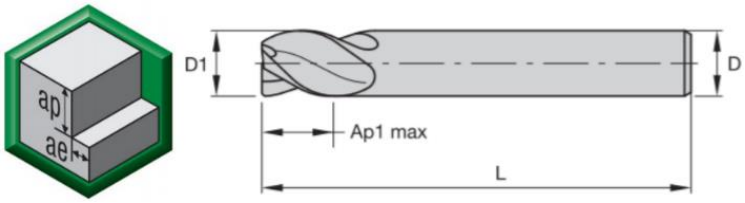

Figure 3. Sketch of milling process and used milling tool [3]

4. SIMULATION RESULTS OF THE THERMAL MODEL

In this chapter a finite element model of DMU40 milling machine using ANSYS software is created. The previously defined boundary conditions, loads, material types, etc. have been assigned tot he model. Then the meshing of the model was generated, then the finite element methods is applied to determine the temperature distributions and to analyse thermal stresses and deformations caused and coupled by thermal and mechanical loads.

It is observed that the maximum temperature appears nearby the contact zones of the milling tool and workpiece. The spindle and further precision units have also loaded by the heat significantly. *Figure 4* shows the effect of cutting temperature during process and temperature field around headstock.

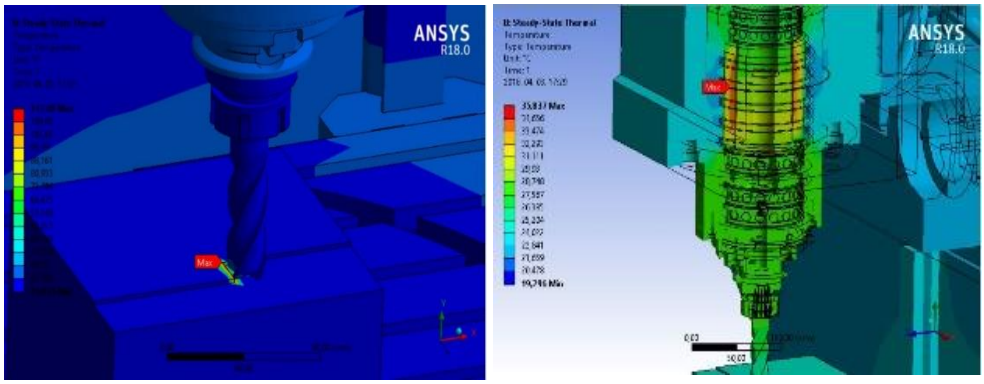

Figure 4. Temperature fields during milling process

Besides, the thermal stress during the milling process was also investigated by the finite element software. We can see that significant stress values can occur around milling tool and workpiece. These effects can dicrease lifecycle of tool and they can reduce quality of product.

Figure 5 shows stress field during process. The deformations in several directions and displacement magnitude were analysed, too. Around milling tool and workpiece there is almost homogeneous deformation field with approximately $60\mu m$ displacement magnitudes. This kind of displacements distribution is advantageous, because we can reduce errors from heat and mechanical effects with easy direct- or indirect compensation algorithms.

Using direct compensation we measure thermal deformations directly with sensors and compensate this errors by modify NC codes of milling process. With indirect compensation algorithms first we create a mathematical thermal model of machine. Combine this model with compensation algorithms we can modify NC codes in real-time during process. Using these methods thermal errors can reduce and accuracy of product can be higher. We can see on *Figure 5* stress field and deformation field during process on machine tool.

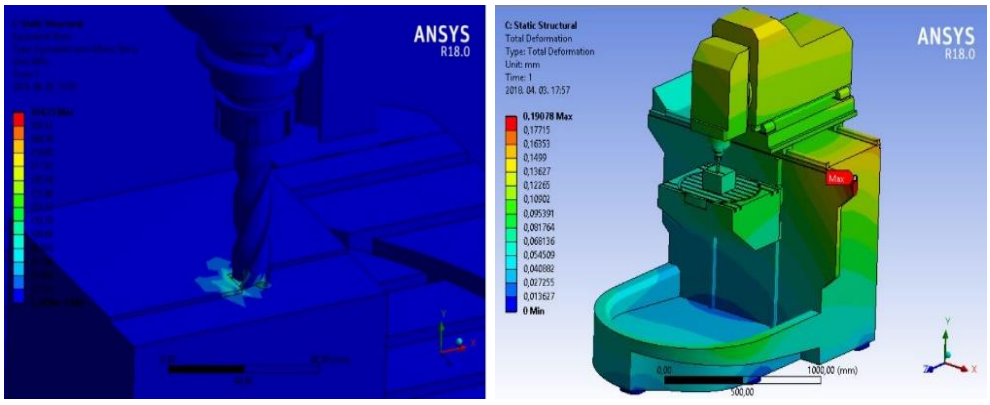

Figure 5. Stress-and deformation fields during milling process

In these figures it is seen that the geometrical 3D model of the machine tool was created as much accuracy as it was necessary, because we wanted to analyse the milling process with real working conditions. A really detailed model however, will increase the calculation time of simulation, and it can be much higher, but the most important is to get a valid simulation first of all.

In this chapter the TCP (Tool Center Point) thermal deformation is also analysed at any working conditions. We used a spindle rotational speed – time function as input parameter. Using ANSYS finite element software we created TCP temperature curve in time and after that I made a simulation series with these parameters. Finally a thermal deformation curve in radial-, and axial directions in time has been obtained. This mathematical model can give a lot of information about milling machine during processes. We can get idea about heat sources, heat conditions, critical structure elements, etc. and it is also possible to draw up some develop directions in machine plannig process.

Figure 6 shows the mentioned mathematical model for TCP thermal deformation.

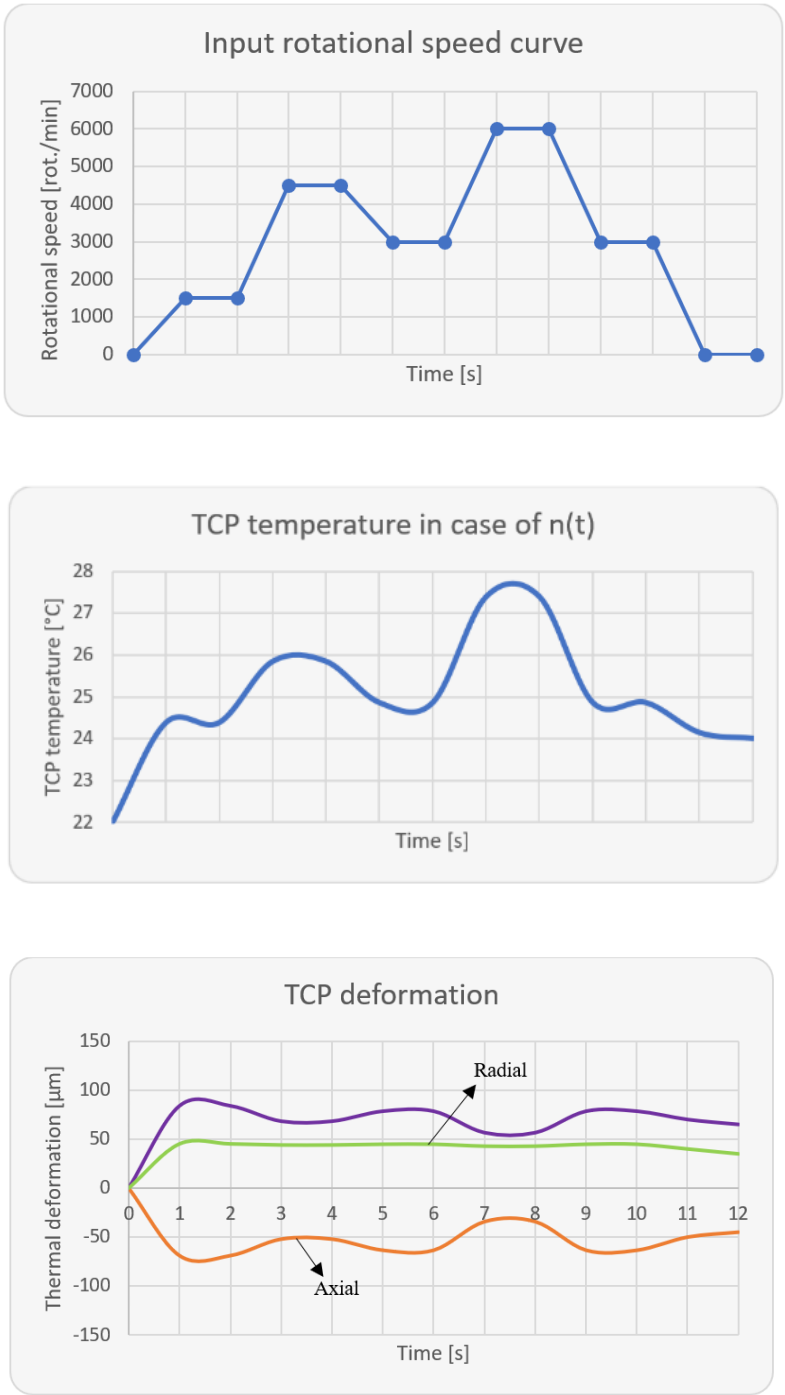

Figure 6. TCP thermal deformation curves used simulation model

5. SUMMARY

In this article an FEM analysis of a 5-axis CNC milling machine during process was performed. First we presented description of temperature fields and warming curves of machine tool units, too. After that we showed a finite element method to solve thermal engineering problems. We created the 3D model of analysed machine tool and we run a complex simulation in ANSYS finite element software. Then the temperature-and stress fields around milling tool and workpiece is presented, besides we also examined displacement fields. and created a mathematical model for TCP thermal deformation in axial and radial directions.

Using these thermal-mechanical analyses we can increase quality of product and reduce thermal errors which can cause geometry inaccuracy in manufactured products. Finite element methods and analysis of machines can also dicrease costs and construction time, so they are really important means at early stage of a designing process.

ACKNOWLEDGEMENT

The described article/presentation/study was carried out as part of the EFOP-3.6.1-16-2016-00011 *Younger and Renewing University – Innovative Knowledge City – institutional development of the University of Miskolc aiming at intelligent specialisation* project implemented in the framework of the Szechenyi 2020 program. The realization of this project is supported by the European Union, co-financed by the European Social Fund.

REFERENCES

[1] Baráti Antal: *Szerszámgép-vizsgálatok*. Budapest, Műszaki Könyvkiadó, 1988.

[2] https://en.dmgmori.com/

[3] https://www.widia.com/en/about-us.html

Design of Machines and Structures, Vol. 9, No. 1 (2019), pp. 54–57.
DOI: 10.32972.dms.2019.006

THERMOVISION ANALYSIS OF A CNC MILLING MACHINE

TAMÁS KUNDRÁT–ATTILA SZILÁGYI

University of Miskolc, Machine Tools and Mechatronics Department
3515 Miskolc-Egyetemváros
kundrattamas@gmail.com
szilagyi.attila@uni-miskolc.hu

Abstract: This article concerns a thermovision analysis of a DMU40 5-axis CNC milling machine [1] using a thermal camera. First I specify the measuring instrument and I present the layout of the measurement. Before this measurement I created a thermal model of machine tool and I analysed it by finite element method. After evaluating simulation results I make the thermovision analysis. Finally I compare measured and simulated results with each other and I draw up some conclusions about thermal analysis.

Keywords: *thermovision analysis, thermal camera, milling machine, compare results, conclusions*

1. PREPARATION OF MEASUREMENT

For preparation I removed possible heat sources from the environment of machine to reduce possible measurement errors. I set an optimal $750\ mm$ distance between object and camera. During the machining process, it is necessary to use coolant, but in my case, this liquid would have greatly distorted the thermal conditions, so the measurement had to be done without it. It was also necessary to open the door closing the machine's work space, as infrared radiation cannot pass through such surfaces (glass, plexiglass). For safety reasons I examined a primitive milling process. The ambient temperature was also checked before the measurement, it was $T_{amb} = 23,3\ °C$. *Figure 1* shows the preparation of measurement the thermal conditions before milling process.

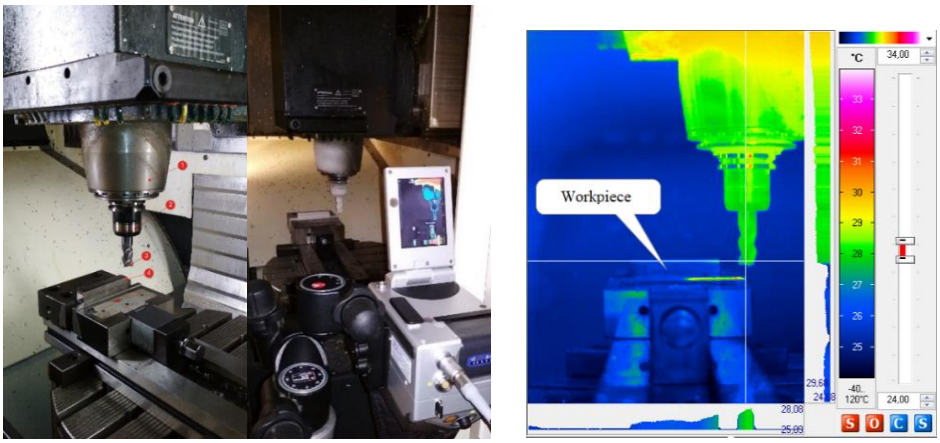

Figure 1. Preparation of measurement, thermal conditions before milling process

2. EVALUATION OF MEASURED RESULT

After the thermovision measurement, I present the results in this chapter and I evaluate them using IRBIS 3 software. During the evaluation first I examined the initial heat conditions. We can see that in Figure 1 at which the spindle operating temperature can be observed. It can be seen that the heat distribution on the spindle and the tool surface can be considered quasi-homogeneous.

Figure 2 shows a quasi-stationary heat state during process and also shows the end of the milling process, where we can see remaining heat loads of tool. They are eventually reduced by using coolant, in order to they will have a quasi-ambient temperature. By using coolant, the heat distribution zone can be limited, the cooling process can be accelerated, thereby reducing the heat load of the tool and increasing its lifecycle.

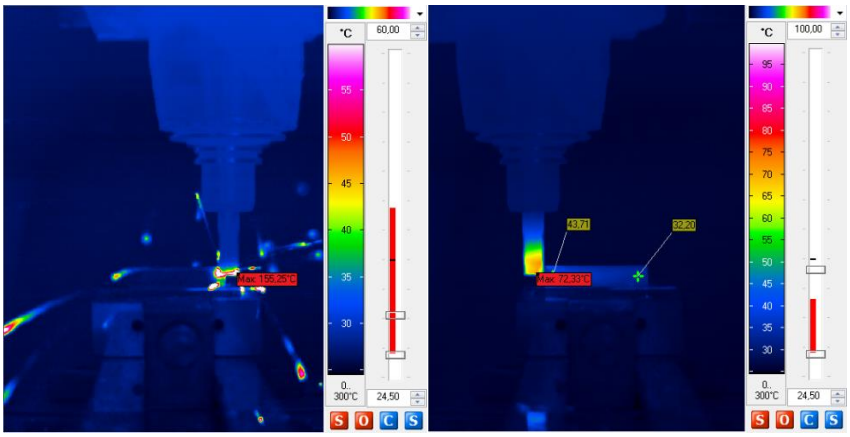

Figure 2. Thermal conditions during and after milling process

2.1. Transient thermal conditions and comparing result

In this section I examine transient thermal conditions of milling process. I also use the IRBIS 3 software to evaluate these results. First I examined the temperature change of the workpiece surface in time. Figure 3 shows the changing of workpiece temperature in process time.

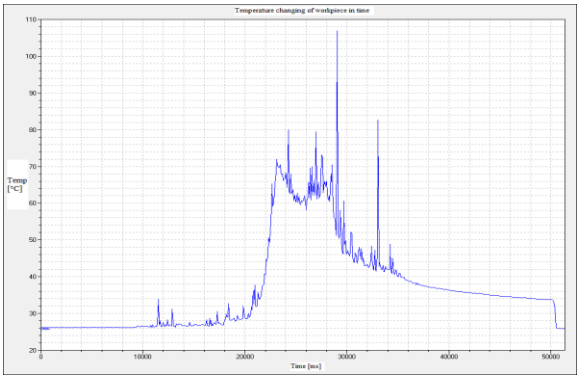

Figure 3. Temperature change of workpiece in time

To do this, I have selected a point on the given surface, and I have created the function for the entire time range while the thermal imager made the recordings. In this time range peaks appear, because of the chips generated by milling process, but they can be eliminated. Thus, a control curve can be fitted to the function, neglecting the influencing factors.

After analyzing the surface of the workpiece, I also examined the maximum values of the temperatures during process. The moment the tool enters, the maximum temperature is suddenly increased. In this case, there are also peaks that can be eliminated like the previous function, because they represent the separated chips, which do not signify directly heat load on the tool or on the workpiece. These temperature values appear at the edges of the tool in the vicinity of the cutting temperatures. So the values previously obtained in the simulation by finite element method are supported by this time diagram, because the heat load I have defined and set in the simulation is close to the average of this measured temperature range. *Figure 4* shows comparing of measured and simulated results.

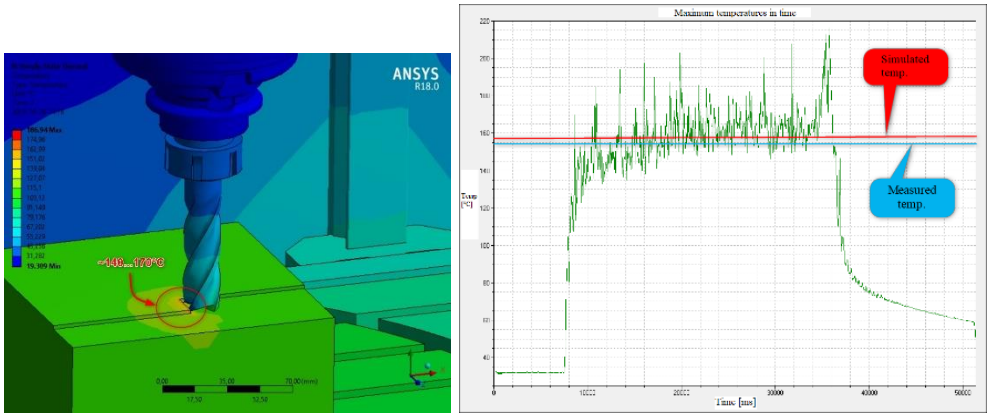

Figure 4. Comparing of the simulated and measured results

By comparing the simulation and measurement results, there was a $\delta \cong 2\%$ error between the results obtained by the two methods. Because of the compicated machine model and complex transient thermal conditions it is a good result of thermal analysis.

The output of the tool is also clearly visible on the chart, whereby the maximum temperature is greatly reduced. In this time range the cooling process curve corresponding to the theoretical cooling curve (exponential character), reaching the equilibrium heat state near the ambient temperature.

3. SUMMARY

In this article was performed a thermovision analysis of a 5-axis CNC milling machine during process. First I presented preparation of measurement and I deatiled the measuring conditions. After that I created the measured results and I used IRBIS 3 software to evaluate them. With the thermal imaging measurements, I was able to compare and support the results of the simulation tools previously used. Among the results obtained with the different methods, only a little $\delta \cong 2\%$ error value appeared, which is a good approximation for the simulation. It has become clear that when examining the case without using coolant, the measured and the simulated results are almost the same, so there is reason to assume that the

thermal imaging measurements would produce similar results, even in the case of using coolant. In addition, it has become evident that even during the design phase or in the manufacturing process, the investigation and treatment of thermal conditions and loads is really important, as they can affect the tool life and may also have a negative impact on the quality of the produced component.

ACKNOWLEDGEMENT

The described article/presentation/study was carried out as part of the EFOP-3.6.1-16-2016-00011 *Younger and Renewing University – Innovative Knowledge City – institutional development of the University of Miskolc aiming at intelligent specialisation* project implemented in the framework of the Szechenyi 2020 program. The realization of this project is supported by the European Union, co-financed by the European Social Fund.

REFERENCES

[1] https://en.dmgmori.com/

Design of Machines and Structures, Vol. 9, No. 1 (2019), pp. 58–63.
DOI: 10.32972.dms.2019.007

EXAMINATION OF DESIGN METHODOLOGY OF SCREW CONVEYORS

KRISTÓF SZABÓ–GYÖRGY TAKÁCS–
GYÖRGY HEGEDŰS–SÁNDOR GERGŐ TÓTH

University of Miskolc, Faculty of Mechanical Engineering and Informatics
Department of Machine Tools
3515 Miskolc-Egyetemváros
szabo.szk@gmail.com
takacs.gyorgy@uni-miskolc.hu
hegedus.gyorgy@uni-miskolc.hu
tothsandorgeri@gmail.com

Abstract: The following article examines the design methodology of screw conveyors. The most significant steps are discussed concerning the design of the apparatus and the use of the tool for machine tools as a service component is explained.

Keywords: *screw conveyor, design theory, methodology*

1. INTRODUCTION

A drastic increase can be perceived in the operation of the production tools so the automation of machining processes requires that the auxiliary processes should be performed automatically by structural units and equipment without direct human intervention [1], [2]. The examination of the design methodology in this article refers to a screw conveyor. Screw handling unit is one of the most used machines with continuous operation with some theoretical questions from János Benkő and Sándor Verdes [3], [4]. The University of Miskolc, Faculty of Mechanical Engineering and Information Technology boasts a wealth of knowledge in the design methodology of various machines and equipment that was utilized in this topic [5], [6], [7], [8].

2. DETERMINATION OF BOUNDARY CONDITIONS

The boundary conditions necessary to start the design phase of the system were defined. The amount of material separated by the machine was determined based on the performance of the milling machine and the maximum applicable size of the tool. During the calculations the maximum allowable cutting speed and feed rate were counted. By multiplying the amount of separated material by the volumetric factor of the chip, the volumetric flow rate of the actual chip volume to be discharged in one minute was obtained. In the case of milling machines, the chip is characterized by a screw, a spiral or a fragmented shape with a volumetric factor of from 3 to 25 [9]. During the designing phase the calculations were executed by using the highest value. The bulk density of the material being transported was determined because it is required to be known to be able to calculate the transport capacity in terms of (tonne per hour).

3. GEOMETRIC SCALING

In case of screw conveyors the geometric scaling of the snail could be determined based on formulas for determining the expected transport capacity and maximum speed [10], which could be described as:

$$D = \sqrt[5]{\left[\frac{240Q}{3{,}6\pi\left(\frac{S}{D}\right)\rho_h \emptyset}\right]^2 \frac{\mu}{2g9{,}55^2\left[cos\delta\sqrt{\mu^2+1}+sin\delta tg(\alpha+\rho)\right]}} \quad (1)$$

The "D" parameter in the equation is the nominal diameter of the screw in meters, the "Q" in the transport capacity ton/hour, the "n" the rev of the worm shaft per minute, the "s" the pitch of the screw spiral in meters, "ρ_h" the bulk density in kg/m^3, "Φ" filling factor, "g" acceleration due to gravity m/s^2, "μ" coefficient of friction, "δ" is the inclination angle of the transport direction in degrees, "ρ" is the angle of friction expressed in degrees, "α" is the pitch angle in degrees, and "s/D" is a standard value. The diameter obtained is the same as the minimum diameter of the screw, which must be multiplied by the safety factor. The obtained result was rounded up to a standard value. By knowing the diameter of the screw conveyor, the minimum speed was calculated as a function of the expected capacity. Being able to determine the proper operating parameters of the material handling unit, the maximum transport capacity at maximum speed should be calculated.

4. DESIGN OF BODY PARTS

During the design of the body elements, mechanical connections to the bed were designed at the first stage. Designing an adapter was necessary as it forms an intermediate element between the machine and the chip carrier, ensuring the proper connection surfaces between the two units. During the design it was so important to seek the proper shaping of the bearing and fixing points. Consideration should be given to the proper support of the auger lines at several points so that the material flow cross-section is reduced to a minimum. It was investigated and identified where the material should be counted, as suitable collecting elements should be placed at appropriate points. If the purpose is the transportation and separation of different states, the appropriate design solutions should be provided to ensure that these functions can be performed during machine operation. Because of the fact that the material is to be collected at one point, the connection of the screws was necessary. A well-designed chamber at the material transfer points was created to ensure a smooth flow of the process. Suitable structural elements were provided for connection to geared motors and ancillary components. The appropriate filtration and collection of the separated liquids was ensured by means of a container. Based on the results of the structural elements, the geometrical and various connection dimensions can be determined. The dimensions of the required length of the screw rows were determined.

5. SELECTION OF STANDARD ELEMENTS

In the following phase, standard parts such as bearings for geared motors and clutches can be selected. In terms of bearing, it is advisable to select from the range of pre-assembled bearing units, however, where the bearings are surrounded by flowing material, it is preferable to choose a plain bearing to utilize the advantageous installation dimensions. To achieve proper operation, in the case of the motors with worm geared motors, it is advisable to select the low

speed and high torque. When selecting the clutch, care must be taken to be able to transfer the power of the drive motor when coupling long axes to be able to tolerate angular defects and reduce harmful dynamic effects.

6. CONTROL

The control of the parts is necessary because it shows whether the parts have been selected correctly. The motors are checked based on the power required to drive each auger line, which depends on static and dynamic loads. The material part added to the trough was considered to be a mass point, and it was assumed that the mass point moves on the surface of the screw base and on the helical edge of the auger, and the factors of friction can be considered to be constant. Thus, starting from the differential equation of the mass point moving on the helical axis [3], the components of forces acting in each direction could be determined as follows:

$$K_x = -N\cos\varphi + B\sin\alpha\sin\varphi \tag{2}$$

$$K_y = -N\sin\varphi - B\sin\alpha\cos\varphi \tag{3}$$

$$K_z = B\cos\alpha \tag{4}$$

Where "N" is the force of the trough wall, "B" is the force exerted on the helical, and "φ" is the angle of rotation of the quasi-permanent state. In addition to the weight of the screw, the bearings are loaded by the same forces as "N" and "B", but the direction is its opposite, so the radial bearing load is:

$$F_r = \sqrt{(N\cos\varphi - B\sin\alpha\sin\varphi)^2 + \left(N\sin\varphi + B\sin\alpha\cos\varphi + G_{csiga}\cos\delta\right)^2} \tag{5}$$

Using the parameters defined so far in *Equation (6)*, the performance which is required to move the material can be determined.

$$P_1 = c\left[K_x v_x + K_y v_y + K_z v_z\right] \tag{6}$$

In the case of the nearly horizontal conveyors, only the z-direction velocity component is not zero, and "c" is a factor that takes internal resistances into account. Determination of the performance requirement of friction:

$$P_2 = \frac{d}{2}\omega(\mu_t F_z + \mu_r F_r) \tag{7}$$

Where "d" stands for the axis diameter, "ω" the circular frequency, "μ_t" is the axial bearing factor of friction, "F" is the axial load force, "μ_r" is the radial bearing factor of friction and "F_r" is the radial load value. The power required to overcome the acceleration resistance plays a role when the material needs to be accelerated from zero, determined by *Equation (8)*.

$$P_3 = Q_{max} v^2 \tag{8}$$

In the equation "Q_{max}" is the maximum transport capacity and "v" is the speed. Based on all the results of the previous calculations, all performance can be calculated as follows:

$$P_{all} = c' \frac{P_1 + P_2 + P_3}{\eta} = [W] \tag{9}$$

In the equation “c” is the safety factor and “η” is the efficiency of the drive. The motors are suitable if their rated power is greater than the power requirement of the screw. The selected clutches were checked at the maximum permissible torque [11]. For plain bearings, the check was based on permissible surface pressure [12].

7. DESIGNING PROCESS

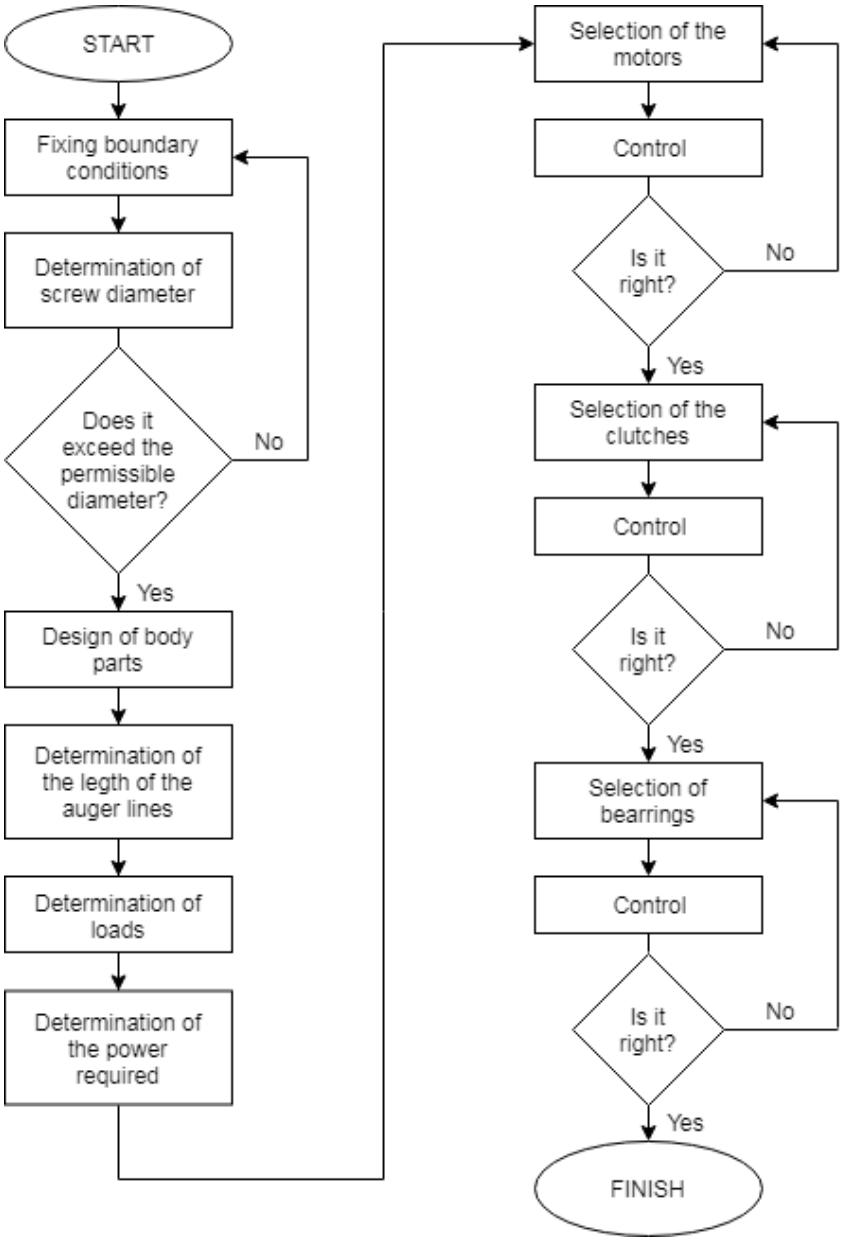

Figure 1. Designing process

8. SUMMARY

The following article demonstrates that the applied design methodology can be used effectively in the design of screw material handling equipment.

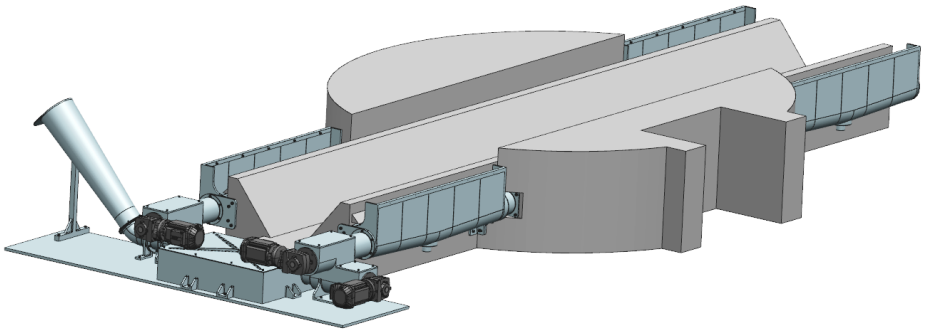

Figure 2. The screw conveyor and the base of the machine

The screw conveyor is shown in *Figure 2* designed on the basis of the design methodology presented in *Figure 1*. The schematic model of the bed of the serviced machine can also be seen in *Figure 2*. The method can be successfully applied to the geometric dimensioning and designing of the screw conveyor. The following method is also suitable if the screw material handling unit is a part of a machine tool. The geometric dimensioning of the structure can be effectively done by the predetermined and fixed boundary conditions. Based on the developed dimensions, the method can be used to accurately determine the static and dynamic loads of the auger lines, which can be used to select and check commercially available standard parts. The use of the design methodology was proved to be successful during the design and control of a universal milling machine's chip conveyor unit in a project.

ACKNOWLEDGEMENT

The described article was carried out as part of the EFOP-3.6.1-16-00011 *Younger and Renewing University – Innovative Knowledge City – institutional development of the University of Miskolc aiming at intelligent specialisation* project implemented in the framework of the Széchenyi 2020 program. The realization of this project is supported by the European Union, co-financed by the European Social Fund.

REFERENCES

[1] Bührdel, Ch.–Frömmer, G.: *Automata forgácsoló szerszámgépek*. Budapest, Műszaki Könyvkiadó, 1984.

[2] Takács Gy.–Szilágyi A.–Demeter P.–Berek A.: *Forgácsoló szerszámgépek*. Budapest, Nemzeti Tankönyvkiadó, 2009.

[3] Benkő J.: Szállítócsigák néhány elméleti kérdése. *Gépgyártástechnológia*, 1994, XXXIV (7–8), pp. 271–282.

[4] Verdes S.: *Anyagmozgatás és gépei*. Veszprém, Pannon Egyetem, 2012.

[5] Szombatfalvy Á.: *Szerkezeti elemek tervezésének technológiai szempontjai*. Budapest, Műszaki Könyvkiadó, 1982, ISBN: 9631037983.

[6] Bercsey T.–Döbröczöni Á.–Dubcsák A.–Horák P.–Kamondi L.–Péter J.–Kelemen G.–Tóth S.: *Terméktervezés- és fejlesztés*. Budapest, PHARE TDQM, 1997.

[7] Kamondi, L.–Sarka, F.–Takács, Á.: *Fejlesztés- módszertani ismeretek*. Miskolc, Nemzeti Tankönyvkiadó, 2011.

[8] Pahl, G.–Beitz, W.–Feldhusen, J.– Grote, K.-H.: *Engineering Design – A Systematic Approach*. London, Springer-Verlag, 2007, ISBN 978-1-84628-318-5.

[9] Kulcsár T.: Gépipari technológiai ismeretek. Veszprém, Pannon Egyetem, 2012.

[10] Benkő J.–Nagy Z.: Tervezési segédlet szállítócsigákhoz, Gödöllő, Szent István Egyetem, 2013.

[11] Németh G.: *Biztonsági tengelykapcsoló méretezése*. Oktatási segédlet, Miskolc, Miskolci Egyetem, 2005.

[12] Péter J.: *Géptervezés alapjai*. Miskolc, Miskolci Egyetemi Kiadó, 2008, 402 old. ISBN 978-963-661-837-7.

Design of Machines and Structures, Vol. 9, No. 1 (2019), pp. 64–67.
DOI: 10.32972.dms.2019.008

GENERATING CONCEPTS WITH MOBILE APPLICATION

ÁGNES TAKÁCS

University of Miskolc, Institute of Machine and Product Design
3515 Miskolc-Egyetemváros
takacs.agnes@uni-miskolc.hu

Abstract: Conceptual design is the first and very important part of the whole design process. This is the phase when the designer engineer analyses on the market existing similar products, complete them with his or her own ideas and generating new solutions. In a lucky situation the designer can generate all the possible solutions of the product. But the whole palette of all the possible solutions usually so extremely huge that a human person cannot look them through. In this case the help of the computer is indispensable. Nowadays rushing world smart phones know everything. There are applications for almost anything even for mechanical engineers to help their everyday routine tasks. In this paper the author makes a suggestion for a mobile application that is suitable for generating concepts of products.

Keywords: *design theory, design methodology, CAxx, mobile App*

1. INTRODUCTION

In previous researches a method has been developed that is capable of generating various solution variants by computer during conceptual design. [1], [2] For applying this method a computer software was developed in a VisualBasic.NET environment. The software generates possible solution variants from the user-defined functional subassemblies using the user-selected mathematical model. The set of solution variants can be narrowed with the help of a user-defined rule system, thus eliminating ineffective or not very promising solution variants. This allows faster evaluation of variations.

In the last years several student tasks have been prepared at the Institute of Machine and Product Design at the University of Miskolc in the topic of design methodology. With these tasks students have learned the basics of conceptual design. Based on their projects, a list has been created that contains frequently recurring functional subassemblies. Thus, the software that was previously created contains a list that further simplifies the user's task: we can choose elements from the existing list of functional subassemblies. With the spread of compact smartphones, simple applications have become useful tools for our everyday life and therefore the study suggests a mobile application.

2. CONCEPTUAL DESIGN

In previous studies and papers Computer Aided methodological Concept Building (or CACB) was introduced [1], [2]. In *Figure 1* logical steps of this method can be seen. Before elaborating the design task, it should be analysed. The tools of this analysis are market research and the investigation of patented solutions. In parallel with that customers' requirements should be found and defined. These requirements should be evaluated and ranked with the designer's eyes, because these are the basis of the evaluation at the end of the concept building method. All the possible functional subassemblies should be defined during the market research and the analysis of patented solutions. Product structures or

solution variants can be generated from these subassemblies. These variants should be evaluated by the designer. The optimal solution that is the result of the concept building is the one that fulfilled all the evaluation criteria.

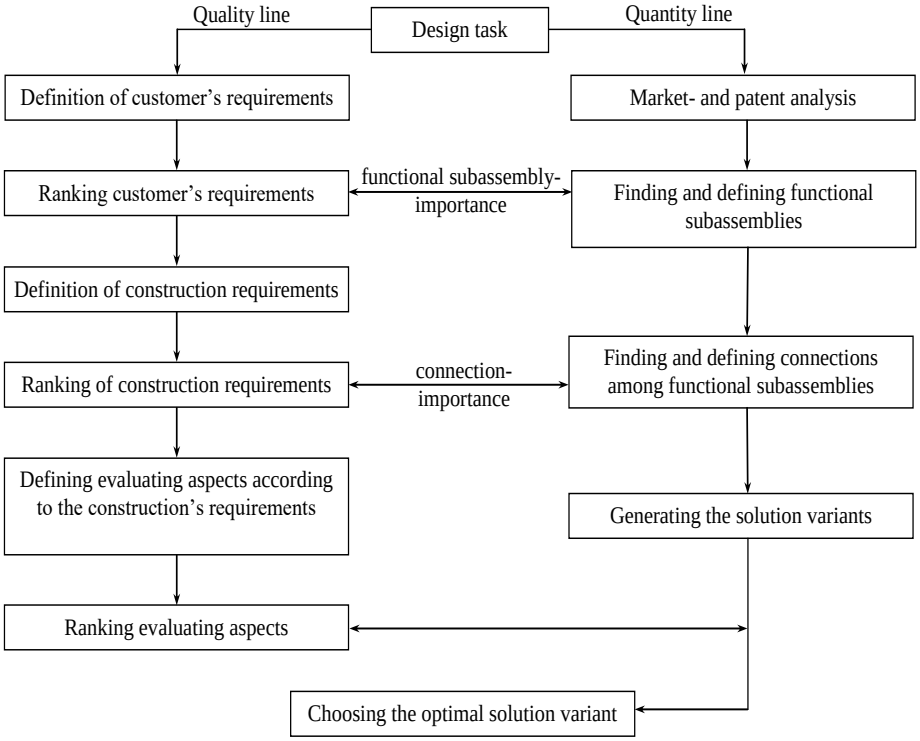

Figure 1. Logical steps of the suggested conceptual design process

Figure 1 [1] focuses on the main scope of previous researches; it summarises the phases of the conceptual design. Suggested method implies a relatively simple algorithm, so the process is adaptable for computer. The introduced method consists of a quantity and a quality line. Quantity line makes it possible the designer could pay attention on more aspects, so more functional subassemblies and this way more solutions. Quality line valuates solutions according to different view-points and tightens the solution-space, optionally for one proper solution. In the modern World of our days it significantly facilitates the task of the engineering designer.

Generating variants can be realized basically in two different ways as it is shown in *Figure 2*; on the basis of the fixed or the flexible functional subassembly set. The worked-out method basically deals with two different theories: solution variants generated by varying the functional subassemblies and solution variants generated by varying the connections among the functional subassemblies. According to *Figure 2* two mathematical solutions for both theories are suggested: the binary logics, and the generation of random numbers. As it is shown in this figure, the different generation theories can show different results. These methods do not eliminate the possibility that the results can fall in with each other.

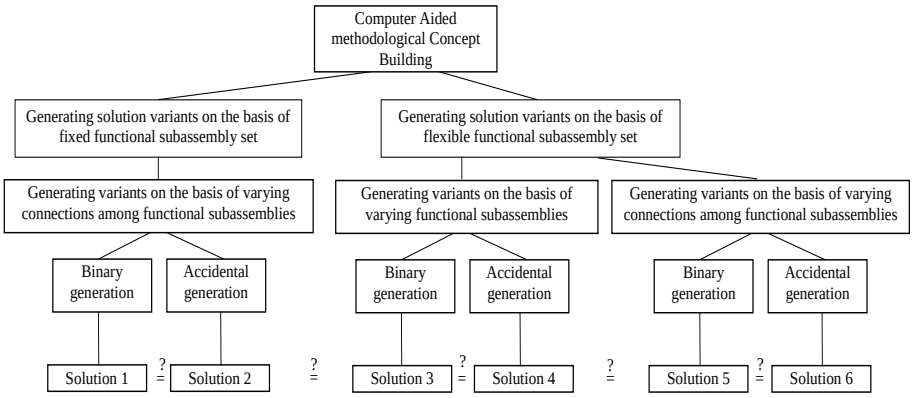

Figure 2. Generating solution variants

3. THE MOBILE APP

The mobile app is being developed in several steps with Google's Android Studio program that can be downloaded free. The first version helps students in the preparation of student projects primarily.

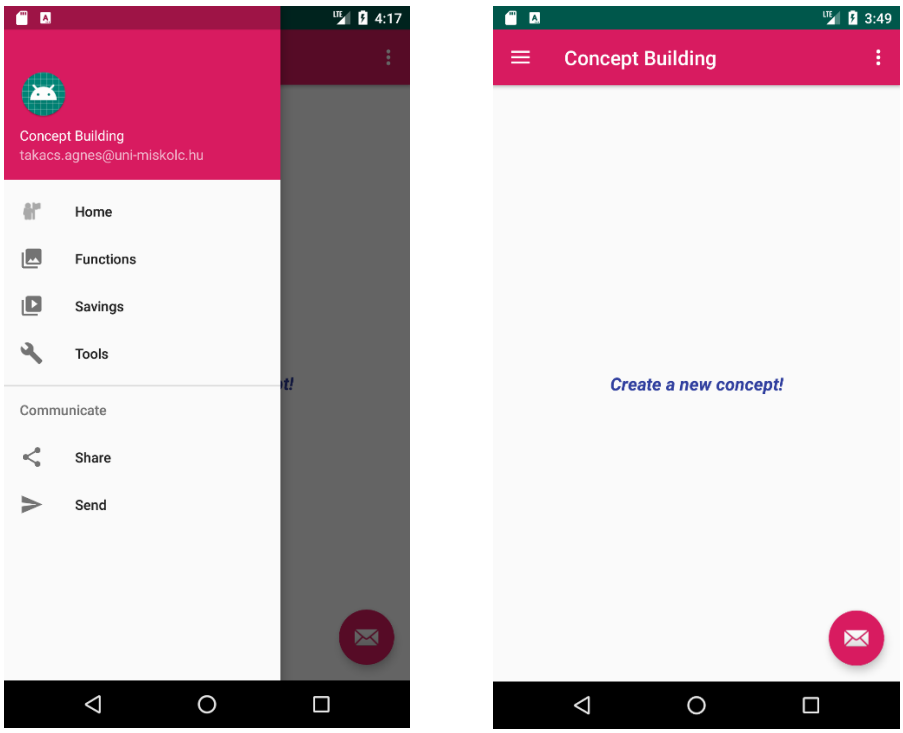

Figure 3. The first visualization of the application

The aim is that the user selects those functional subassemblies from the list of built-in functional subassemblies based on previous tasks that can be considered in the perspective of his/her project and from these functional subassemblies the user can create different product concepts. Each built-in functional subassembly has an icon that the user can drag into the image editing area of the application (right hand side of the *Figure 3*). If the user has selected all the necessary functional subassemblies, then by inserting line elements he/she can create different solution variants. The user can save them as a picture on his/her mobile device.

There is also the possibility to use templates some typical often occurring structure graphs can be found in the application. In this case, the user should only drag the icon of the required functional subassembly in the correct position. This concept can be expanded with additional elements and can also be saved on the device. *Figure 3* illustrates the visualization of the application.

4. SUMMARY

The conceptual design phase, in comparison with the other steps of the whole design process is barely supported by computer. The research intends to fill this gap. The most important aspect is to help brainstorming with an easy-to-use application on mobile devices. In the first phase of the research, the aim is that the students use the application in their own individual tasks in design methodology lessons and build concepts based on their individual ideas. A further goal is to create a version of the application that is capable of generating all the possible solution variants from functional subassemblies selected by the user and then reducing the large number of solutions based on the user-defined rule set, according to the theory in chapter 2 of this article.

ACKNOWLEDGEMENT

The described article/presentation/study was carried out as part of the EFOP-3.6.1-16-2016-00011 *Younger and Renewing University – Innovative Knowledge City – institutional development of the University of Miskolc aiming at intelligent specialization* project implemented in the framework of the Szechenyi 2020 program. The realization of this project is supported by the European Union, co-financed by the European Social Fund.

REFERENCES

[1] Takács Á: *Számítógéppel segített koncepcionális tervezési módszer.* PhD-disszertáció, Miskolc, 2010.

[2] Takács, Á: Computer Aided Concept Building. *Solid State Phenomena*, Vol. 261. Trans Tech Publications, Switzerland, 2017, ISSN 1662-9779.

[3] Pahl, G.–Beitz, W.: Engineering Design – A Systematic Approach. London, Springer Verlag, 2005, ISBN 3-540-19917.

[4] Otto, K.–Wood, K.: *Product Design – Techniques in Reverse Engineering and New Product Development*. Prentice Hall, 2008, ISBN 0-13-021271-7.

REVIEWING COMMITTEE

P. BENCS	Department of Fluid and Heat Engineering Institute of Energy Engineering and Chemical Machinery H-3515 Miskolc-Egyetemváros, Hungary arambp@uni-miskolc.hu
CS. DÖMÖTÖR	Institute of Machine- and Product Design University of Miskolc H-3515 Miskolc-Egyetemváros, Hungary machdcs@uni-miskolc.hu
GY. HEGEDŰS	Institute of Machine Tools and Mechatronics University of Miskolc H-3515 Miskolc-Egyetemváros, Hungary hegedus.gyorgy@uni-miskolc.hu
F. SARKA	Institute of Machine and Product Design University of Miskolc H-3515 Miskolc-Egyetemváros, Hungary machsf@uni-miskolc.hu
A. SZILÁGYI	Institute of Machine Tools and Mechatronics University of Miskolc H-3515 Miskolc-Egyetemváros, Hungary szilagyi.attila@uni-miskolc.hu
F. SZABÓ	Institute of Machine and Product Design University of Miskolc H-3515 Miskolc-Egyetemváros, Hungary machszf@uni-miskolc.hu
L. G. SZEPESI	Institute of Energy Engineering and Chemical Machinery H-3515 Miskolc-Egyetemváros, Hungary szepesi@uni-miskolc.hu
Á. TAKÁCS	Institute of Machine and Product Design University of Miskolc H-3515 Miskolc-Egyetemváros, Hungary takacs.agnes@uni-miskolc.hu

Secreteriat of the Vice-Rector for Research and International Relations,
University of Miskolc,
Responsible for the Publication: Prof. dr. Tamás Kékesi
Published by the Miskolc University Press under leadership of Attila Szendi
Responsible for duplication: Erzsébet Pásztor
Editor: Dr. Ágnes Takács
Technical editor: Csilla Gramantik
Proofreader: Zoltán Juhász
Number of copies printed: 58
Put the Press in 2019
Number of permission: TNRT–2019– 180 –ME
HU ISSN 1785-6892 in print
HU ISSN 2064-7522 online